Inorg. Chem. **2007**, *46*, 4997–5012

Fast O_2 Binding at Dicopper Complexes Containing Schiff-Base Dinucleating Ligands

Anna Company,[†] Laura Gómez,[†] Rubén Mas-Ballesté,[‡] Ivan V. Korendovych,[§] Xavi Ribas,[†] Albert Poater,[†] Teodor Parella,[||] Xavier Fontrodona,[⊥] Jordi Benet-Buchholz,[#] Miquel Solà,*[,†] Lawrence Que, Jr.,*[,‡] Elena V. Rybak-Akimova,*[,§] and Miquel Costas*[,†]

Departament de Química and Institut de Química Computacional, Universitat de Girona, Campus de Montilivi E-17071, Girona, Spain, Department of Chemistry and Center for Metals in Biocatalysis, University of Minnesota, Minneapolis, Minnesota 55455, USA, Department of Chemistry, Tufts University, Medford, Massachusetts 02155, Servei de RMN, Universitat Autònoma de Barcelona, Bellaterra, E-08193 Barcelona, Spain, Institute of Chemical Research of Catalonia (ICIQ) E-43007 Tarragona, Spain, and Serveis Científico-Tècnics, Universitat de Girona, Campus de Montilivi, E-17071, Girona, Spain

Received January 22, 2007

A new family of dicopper(I) complexes $[Cu^{I}_2{}^{R}L](X)_2$ (R = H, **1X**, R = ^{t}Bu, **2X** and R = NO_2, **3X**, X = CF_3SO_3, ClO_4, SbF_6, or BArF, BArF = $[B\{3,5\text{-}(CF_3)_2C_6H_3\}_4]^-$), where ^{R}L is a Schiff-base ligand containing two tridentate binding sites linked by a xylyl spacer, has been prepared and characterized, and its reaction with O_2 has been studied. The complexes were designed with the aim of reproducing structural aspects of the active site of type 3 dicopper proteins; they contain two three-coordinate copper sites and a rather flexible podand ligand backbone. The solid-state structures of **1ClO$_4$**, **2CF$_3$SO$_3$**, **2ClO$_4$**, and **3BArF·CH$_3$CN** have been established by single-crystal X-ray diffraction analysis. **1ClO$_4$** adopts a polymeric structure in the solid state while **2CF$_3$SO$_3$**, **2ClO$_4$**, and **3BArF·CH$_3$CN** are monomeric. The complexes have been studied in solution by means of ^{1}H and ^{19}F NMR spectroscopy, which put forward the presence of dynamic processes. **1**–**3BArF** and **1**–**3CF$_3$SO$_3$** in acetone react rapidly with O_2 to generate metaestable $[Cu^{III}_2(\mu\text{-}O)_2(^{R}L)]^{2+}$ **1**–**3(O$_2$)** and $[Cu^{III}_2(\mu\text{-}O)_2(CF_3SO_3)(^{R}L)]^{+}$ **1**–**3(O$_2$)(CF$_3$SO$_3$)** species, respectively, that have been characterized by UV–vis spectroscopy and resonance Raman analysis. Instead, reaction of **1**–**3BArF** with O_2 in CH_2Cl_2 results in intermolecular O_2 binding. DFT methods have been used to study the chemical identities and structural parameters of the O_2 adducts, and the relative stability of the $Cu^{III}_2(\mu\text{-}O)_2$ form with respect to the $Cu^{II}_2(\mu\text{-}\eta^2\text{:}\eta^2\text{-}O_2)$ isomer. The reaction of **1X**, X = CF_3SO_3 and BArF, with O_2 in acetone has been studied by stopped-flow UV-vis exhibiting an unexpected very fast reaction rate ($k = 3.82(4) \times 10^3$ M^{-1} s^{-1}, $\Delta H^{\ddagger} = 4.9 \pm 0.5$ kJ·mol^{-1}, $\Delta S^{\ddagger} = -148 \pm 5$ J·K^{-1}·mol^{-1}), nearly 3 orders of magnitude faster than in the parent $[Cu^{I}_2(\text{m-XYL}^{\text{MeAN}})]^{2+}$. Thermal decomposition of **1**–**3(O$_2$)** does not result in aromatic hydroxylation. The mechanism and kinetics of O_2 binding to **1X** (X = CF_3SO_3 and BArF) are discussed and compared with those associated with selected examples of reported models of O_2-processing copper proteins. A synergistic role of the copper ions in O_2 binding and activation is clearly established from this analysis.

Introduction

Tyrosinase, catechol oxidase, and hemocyanin constitute prototypical cases of proteins capable of activating or transporting O_2 through a synergistic actuation of two copper ions.[1,2] Interestingly, a recent crystallographic study on tyrosinase shows a remarkably flexible dicopper binding site where the Cu···Cu distance undergoes large changes along its catalytic cycle, in order to accommodate the bridging molecule.[3] These proteins inspired the work of many research groups, which have focused their investigation on studying

* To whom correspondence should be addressed. E-mail: miquel.costas@udg.es (M.C.).
[†] Departament de Química and Institut de Química Computacional, Universitat de Girona.
[‡] University of Minnesota.
[§] Tufts University.
[||] Universitat Autònoma de Barcelona.
[⊥] Servei d'Anàlisi Química, Universitat de Girona.
[#] Institute of Chemical Investigation of Catalonia.

(1) Solomon, E. I.; Sundaram, U. M.; Machonkin, T. E. *Chem. Rev.* **1996**, *96*, 2563−2605.
(2) Solomon, E. I.; Chen, P.; Metz, M.; Lee, S.-K.; Palmer, A. E. *Angew. Chem., Int. Ed.* **2001**, *40*, 4570−4590.

10.1021/ic0701108 CCC: $37.00
Published on Web 05/15/2007

Scheme 1

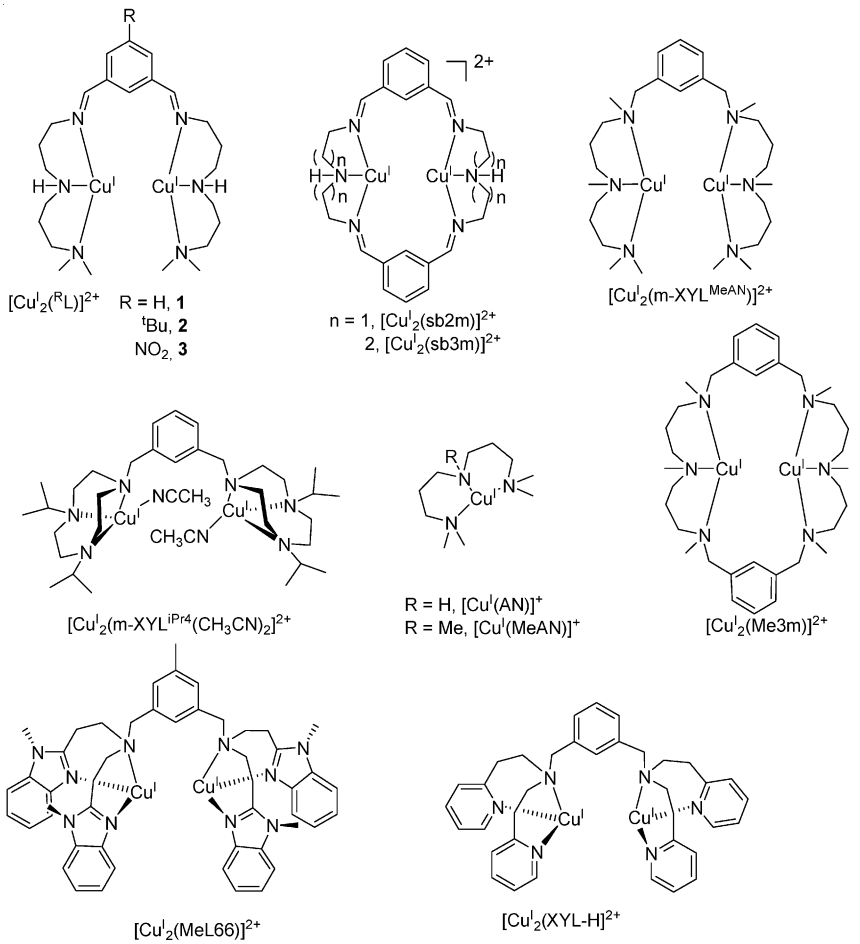

dioxygen binding and/or activation by synthetic copper complexes.[4−7] Establishing the fundamental mechanisms by which a dicopper site binds and/or activates O_2 has proven to be a formidable task still far from being understood. To date, most of the studies with model complexes rely on the use of mononuclear copper complexes that spontaneously self-assemble into a binuclear core upon exposure to O_2. A different strategy based on the design of binucleating ligands has been developed in order to evaluate putative cooperative effects between the copper centers.[4−8] Along this path, we have recently studied the O_2 chemistry of dicopper(I) complexes containing podand $[Cu^I_2(m\text{-}XYL^{MeAN})]^{2+}$ and macrocyclic $[Cu^I_2(Me3m)]^{2+}$ structures (see Scheme 1), both of which share electronic and structural features of their metal binding sites, and we have demonstrated that the more flexible podand structure exhibits remarkably faster O_2 reactivity, arising from a synergistic actuation of the two copper ions.[9]

In this work we have designed and prepared a new family of dicopper(I) complexes containing podand-type Schiff-base ligands (Scheme 2), which bear structural resemblance to previously described macrocyclic ligands,[10] and we have studied their reactivity with dioxygen. The O_2 chemistry of related macrocyclic dicopper complexes $[Cu^I_2(L)]^{2+}$, L = sb2m and sb3m (Scheme 1), has been previously studied, but no O_2-adducts were detected.[10−17] In an attempt to model type 3 active sites, important aspects of our design are the N_3 coordination environment of the copper ions and a rather flexible ligand scaffold. Despite including rather soft imine ligands, which tend to stabilize the cuprous oxidation state,

(3) Matoba, Y.; Kumagai, T.; Yamamoto, A.; Yoshitsu, H.; Sugiyama, M. *J. Biol. Chem.* **2006**, *281*, 8981−8990.
(4) Lewis, E. A.; Tolman, W. B. *Chem. Rev.* **2004**, *114*, 1047−1076.
(5) Mirica, L. M.; Ottenwaelder, X.; Stack, T. D. P. *Chem. Rev.* **2004**, *114*, 1013−1046.
(6) Hatcher, L. Q.; Karlin, K. D. *J. Biol. Inorg. Chem.* **2004**, *9*, 669−683.
(7) Schindler, S. *Eur. J. Inorg. Chem.* **2000**, 2311−2326.
(8) Battaini, G.; Granata, A.; Monzani, E.; Gullotti, M.; Casella, L. *Adv. Inorg. Chem.* **2006**, *58*, 185−233.
(9) Company, A.; Lamata, D.; Poater, A.; Solà, M.; Llobet, A.; Parella, T.; Fontrodona, X.; Que, L., Jr.; Costas, M. *Inorg. Chem.* **2006**, *45*, 5239−5241.
(10) Utz, D.; Heinemann, F. W.; Hampel, F.; Richens, D. T.; Schindler, S. *Inorg. Chem.* **2003**, *42*, 1430−1436.
(11) Menif, R.; Martell, A. E. *J. Chem. Soc., Chem. Commun.* **1989**, *20*, 1521−1523.
(12) Menif, R.; Martell, A. E.; Squattrito, P. J.; Clearfield, A. *Inorg. Chem.* **1990**, *29*, 4723−4729.
(13) Rockcliffe, D. A.; Martell, A. E. *J. Chem. Soc., Chem. Commun.* **1992**, 1758−1760.
(14) Rockcliffe, D. A.; Martell, A. E. *Inorg. Chem.* **1993**, *32*, 3143−3152.
(15) Martell, A. E.; Motekaitis, R. J.; Menif, R.; Rockcliffe, D. A.; Llobet, A. *J. Mol. Catal. A: Chem.* **1997**, *117*, 205−213.
(16) Llobet, A.; Martell, A. E.; Martínez, M. A. *J. Mol. Catal. A: Chem.* **1998**, *129*, 19−26.
(17) Ryan, S.; Adams, H.; Fenton, D. E.; Becker, M.; Schindler, S. *Inorg. Chem.* **1998**, *37*, 2134−2140.

Scheme 2. Syntheses of Ligands ^{R}L and Complexes $[Cu^{I}_2(^{R}L)]X_2$

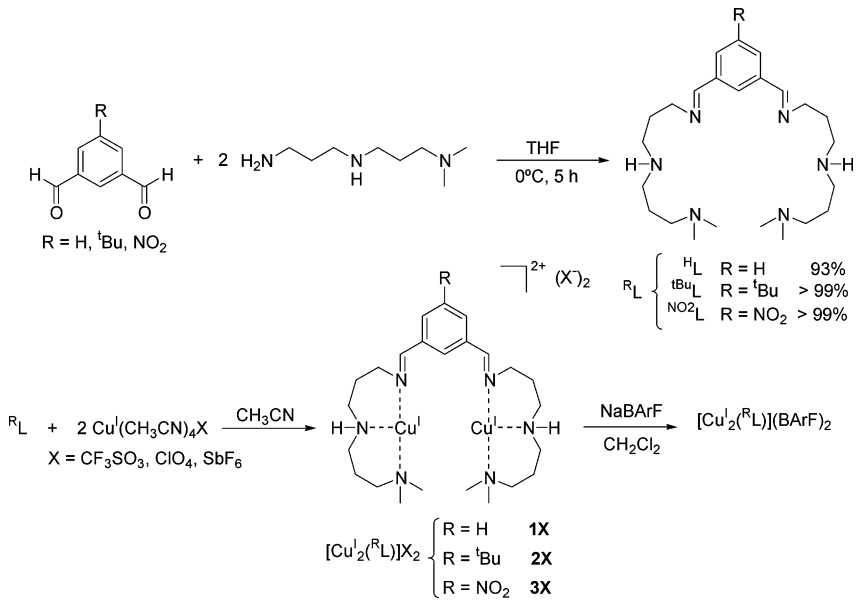

the complexes prepared in this work exhibit remarkably fast O_2 binding. Spectroscopic and computational studies on the nature of the metastable oxygenated intermediates formed along this reaction demonstrate that their structure and nuclearity depend on solvent and counterions. Kinetic parameters for O_2 binding/reduction are also studied and compared with those of selected synthetic complexes that model O_2-processing copper proteins.

Experimental Section

Caution: Perchlorate salts are all potentially explosive and should be handled with care.

Materials and Synthesis. Reagent-grade solvents were purchased from SDS. Diethyl ether and THF were distilled over Na/benzophenone. Acetonitrile and CH_2Cl_2 were distilled over CaH_2, and acetone was dried over $CaCl_2$. Solvents were degassed by several Ar−vacuum cycles and stored in an anaerobic glove box over molecular sieves. Unless noted otherwise, all reagents were purchased from commercial sources and used as received. Preparation and handling of air-sensitive materials were carried out under argon or N_2 atmosphere using standard Schlenk techniques or in a N_2-filled anaerobic box ($[O_2] < 1$ ppm, $[H_2O] < 1$ ppm).

5-*tert*-Butylbenzene-1,3-dicarbaldehyde[18] and $[Cu^{I}(CH_3CN)_4]X$ (X = ClO_4, CF_3SO_3, and SbF_6) were prepared according to published procedures or slight modifications thereof.[19,20]

Ligand Synthesis. 5-Nitrobenzene-1,3-dicarbaldehyde. Benzene-1,3-dialdehyde (2.0 g, 15 mmol) was dissolved in H_2SO_4 98% (6.5 mL) and cooled at 0 °C in an ice bath. A mixture of H_2SO_4 98% (2 mL) and HNO_3 65% (4 mL) was added dropwise to the stirred solution which was then warmed at 50 °C for an hour. The crude mixture was poured onto ice which caused the formation of a precipitate which was filtered off and washed with water and diethyl ether. The resulting pale yellow solid was dried under vacuum giving 1.98 g of the desired compound (11 mmol, 73%). Anal. Calcd for $C_8H_5NO_4$ (MW = 179.13 g·mol^{-1}): N, 7.82; C, 53.64; H, 2.81%. Found: N, 7.46; C, 53.13; H, 2.84%. FT-IR (ATR) ν, cm^{-1}: 1695 (C═O), 1537, 1346 (NO_2). ^{1}H NMR (200 MHz, $CDCl_3$, 300 K) δ, ppm: 10.21 (s, 2H, C**H**O), 8.96 (s, 2H, Ar**H**), 8.72 (s, 1H, Ar**H**). ^{13}C NMR (50 MHz, $CDCl_3$, 300 K) δ, ppm: 188.37 (**C**HO), 138.24 (ar$\mathbf{C_q}$−NO_2), 134.46 (ar$\mathbf{C_q}$−CHO), 128.47 (ar**C**−H). GC-MS (*m*/*z*): 179.0 (100).

Synthesis of ^{R}L, R = H, ^{t}Bu and NO_2 were prepared by the same method, as exemplified for ^{H}L.

Synthesis of ^{H}L. A solution of *N*,*N*-dimethyldipropylenetriamine (3.6 mL, 20 mmol) in THF (40 mL) was cooled in an ice bath at 0 °C, and a solution of benzene-1,3-dialdehyde (1.34 g, 10 mmols) in THF (20 mL) was added dropwise under vigorous stirring. The mixture was left to attain room temperature, and it was stirred for an additional 5 h. Then, the solvent was removed under reduced pressure, and the resultant product was dried under vacuum to obtain 3.87 g (9.3 mmol, 93%) of a yellow oil corresponding to **^{H}L**. Anal. Calcd for $C_{24}H_{44}N_6\cdot 1/3H_2O$ (MW = 422.65 g·mol^{-1}): N, 19.88; C, 68.20; H, 10.65%. Found: N, 19.98; C, 68.30; H, 10.54%. FT-IR (ATR) ν, cm^{-1}: 2940 − 2723 (C−H)$_{sp3}$, 1648 (C═N), 1460 (C═C$_{ar}$). ^{1}H NMR ($CDCl_3$, 200 MHz, 298 K) δ, ppm: 8.31, 8.27, 7.75−7.64, 7.49−7.28, 3.98−3.90, 3.76−3.66, 3.33−3.09, 2.75−2.66, 2.35−2.28, 2.21−2.12, 1.92−1.82, 1.66−1.52. ^{13}C NMR ($CDCl_3$, 50 MHz, 300 K) δ, ppm: 160.88, 142.97, 142.85, 142.56, 136.53, 129.49, 128.80, 127.40, 127.31, 127.00, 126.43, 126.02, 81.82, 81.63, 81.54, 67.89, 59.74, 58.03, 57.79, 57.68, 52.19, 52.09, 51.86, 51.74, 51.50, 48.38, 48.00, 45.62, 45.49, 45.37, 45.34, 28.07, 27.29, 26.84, 25.554, 24.78, 24.53. The assignment of the NMR spectra of **^{H}L** is complicated due to the existence of an equilibrium between different isomers in solution. ESI-MS (*m*/*z*): 417.0 (100) $[M + H]^+$.

Synthesis of ^{tBu}L resulted in 2.46 g (5.2 mmol, > 99%) of a yellow oil corresponding to **^{tBu}L**. Anal. Calcd for $C_{28}H_{52}N_6\cdot 1.5H_2O$ (MW = 499.77 g·mol^{-1}): N, 16.82; C, 67.29; H, 11.09%. Found: N, 16.33; C, 67.35; H, 11.25%. FT-IR (ATR) ν, cm^{-1}: 3285 (N−H), 2940−2765 (C−H)$_{sp3}$, 1647 (C═N), 1459 (C═C$_{ar}$). ^{1}H NMR ($CDCl_3$, 200 MHz, 300 K) δ, ppm: 8.27, 7.67, 7.55−7.52, 7.34, 3.95−3.89, 3.66, 3.27−3.10, 2.82−2.68, 2.36−2.07, 1.93−1.85, 1.66−1.63, 1.34−1.32. ^{13}C NMR ($CDCl_3$, 50 MHz, 300 K) δ, ppm: 161.47, 151.73, 142.44, 136.22, 126.57, 124.85, 124.35,

(18) Bennani, Y. L.; Marron, K. S.; Mais, D. E.; Flatten, K.; Nadzan, A. M.; Boehm, M. F. *J. Org. Chem.* **1998**, *63*, 543−550.
(19) Kubas, G. J. *Inorg. Synth.* **1979**, *19*, 90−92.
(20) Kubas, G. J. *Inorg. Synth.* **1990**, *28*, 68−70.

123.92, 82.14, 81.94, 67.90, 59.74, 58.04, 57.93, 52.21, 51.82, 48.48, 47.90, 45.70, 45.47, 45.38, 40.55, 34.76, 33.26, 31.41, 31.07 27.89, 27.60, 27.37, 27.11, 25.55, 24.73. ESI-MS (*m*/*z*): 473.5 (100) $[M + H]^+$.

Synthesis of ^{NO2}L resulted in 4.41 g (9.6 mmol, >99%) of a yellow oil corresponding to ^{NO2}**L**. Anal. Calcd for $C_{24}H_{43}N_7O_2 \cdot 2H_2O$ (MW = 488.67 g·mol^{-1}): N, 19.70; C, 57.92; H, 9.52%. Found: N, 20.06; C, 57.97; H, 9.82%. FT-IR (ATR) ν, cm^{-1}: 2940−2782 $(C-H)_{sp3}$, 1645 (C═N), 1531, 1343 (NO_2), 1460 ($C═C_{ar}$). ^{1}H NMR ($CDCl_3$, 200 MHz, 300 K) δ, ppm: 8.27, 7.67, 7.55−7.52, 7.34, 4.09−4.04, 3.09, 2.82−2.65, 2.36−2.29, 1.12, 2.03−1.97, 1.88−1.85, 1.66−1.55. ^{13}C NMR ($CDCl_3$, 50 MHz, 300 K) δ, ppm: 148.71, 145.08, 144.86, 133.08, 132.92, 121.92, 80.56, 80.25, 67.87, 57.99, 57.62, 51.75, 51.64, 51.44, 51.33, 48.36, 47.85, 45.43, 45.35, 40.51, 32.98, 27.44, 26.78, 26.26, 25.53, 24.87, 24.76. ESI-MS (*m*/*z*): 462.5 (100) $[M + H]^+$.

Syntheses of Complexes. $[Cu^I_2(^RL)](CF_3SO_3)_2$, $[Cu^I_2(^RL)](ClO_4)_2$, and $[Cu^I_2(^RL)](SbF_6)_2$ (R = H, ^{t}Bu, NO_2) were prepared by the same method, starting from the particular ligand, as exemplified for **1CF$_3$SO$_3$**.

$[Cu^I_2(^HL)](CF_3SO_3)_2$, 1CF$_3SO_3$. ^{H}**L** (82 mg, 0.20 mmol) was dissolved in CH_3CN (1 mL), and $[Cu^I(CH_3CN)_4]CF_3SO_3$ (148 mg, 0.39 mmol) was added directly as a solid into the vigorously stirred solution, generating a deep orange-red solution. After 30 min, the resulting solution was filtered through Celite. Slow diethyl ether diffusion afforded the desired compound as an orange solid which was dried under vacuum (134 mg, 0.16 mmol, 81%). Anal. Calcd for $C_{26}H_{44}Cu_2F_6N_6O_6S_2$ (MW = 841.88 g·mol^{-1}): N, 9.98; C, 37.09; H, 5.27; S, 7.62%. Found: N, 9.64; C, 36.98; H, 5.23; S, 7.31%. FT-IR (ATR) ν, cm^{-1}: 3247 (N−H), 2924−2868 $(C-H)_{sp3}$, 1628 (C═N), 1466 ($C═C_{ar}$), 1248, 1152, 1027, 634, 516 (CF_3SO_3). ^{1}H NMR (D_6-acetone, 200 MHz, 300 K) δ, ppm: 8.73 (s, 2H, N═C**H**), 8.60 (s, 1H, Ar**H**), 8.36 (d, 2H, J = 7.6 Hz, Ar**H**), 7.84 (t, 1H, J = 7.6 Hz, Ar**H**), 4.13 (s broad, 4H, HC═N−C**H**$_2$), 3.57−2.75 (m, 12H, N-**C**H$_2$−C), 2.54 (s broad, 12H, N−C**H**$_3$), 2.01−1.70 (m, 8H, C−C**H**$_2$−C). ^{1}H NMR (CD_2Cl_2, 200 MHz, 300 K) δ, ppm: 8.64 (s, 1H, Ar**H**), 8.51 (s, 2H, N═C**H**), 8.14 (d, 2H, J = 7.6 Hz, Ar**H**), 7.69 (t, 1H, J = 7.6 Hz, Ar**H**), 4.05 (s broad, 4H, HC═N−C**H**$_2$), 3.47−3.17 (m, 6H, N−**C**H$_2$−C), 2.99−2.60 (m, 6H, N−**C**H$_2$−C), 2.45 (s broad, 12H, N−C**H**$_3$), 2.15−1.69 (m, 8H, C−C**H**$_2$−C).

$[Cu^I_2(^HL)](ClO_4)_2$, 1ClO$_4$. (98% Yield.) Anal. Calcd for $C_{24}H_{44}Cl_2Cu_2N_6O_8$ (MW = 742.64 g·mol^{-1}): N, 11.32 C, 38.82; H, 5.97%. Found: N, 11.38; C, 38.89; H, 6.12%. FT-IR (ATR) ν, cm^{-1}: 3271 (N−H), 2929−2865 $(C-H)_{sp3}$, 1627 (C═N), 1468 ($C═C_{ar}$), 1073, 621 (ClO_4). UV−vis (CH_2Cl_2) λ_{max}, nm (ϵ, M^{-1} cm^{-1}): 231 (29000), 291 (6800), 412 (1700).

$[Cu^I_2(^HL)](SbF_6)_2$, 1SbF$_6$. (81% Yield.) Anal. Calcd for $C_{24}H_{44}Cu_2F_{12}N_6Sb_2$ (MW = 1015.24 g·mol^{-1}): N, 8.28; C, 28.39; H, 4.37%. Found: N, 8.16; C, 28.35; H, 4.68%. FT-IR (ATR) ν, cm^{-1}: 2933−2871 $(C-H)_{sp3}$, 1626 (C═N), 1463 ($C═C_{ar}$), 653 (SbF_6). ^{1}H NMR (D_6-acetone, 200 MHz, 300 K) δ, ppm: 8.72 (s, 2H, N═C**H**), 8.50 (d, 2H, J = 7.6 Hz, Ar**H**), 8.38 (s, 1H, Ar**H**), 7.94 (t, 1H, J = 7.6 Hz, Ar**H**), 4.16 (s broad, 4H, HC═N−C**H**$_2$), 3.34−2.76 (m. broad, 12H, N−C**H**$_2$−C), 2.62 (s broad, 12H, N−C**H**$_3$), 2.02−1.71 (m, 8H, C−C**H**$_2$−C).

$[Cu^I_2(^{tBu}L)](CF_3SO_3)_2$, 2CF$_3SO_3$. (74% Yield.) Anal. Calcd for $C_{30}H_{52}Cu_2F_6N_6O_6S_2 \cdot 1H_2O$ (MW = 916.00 g·mol^{-1}): N, 9.17; C, 39.34; H, 5.94; S, 7.00%. Found: N, 9.52; C, 39.15; H, 6.20; S, 6.76%. FT-IR (ATR) ν, cm^{-1}: 3249 (N−H), 2961−2872 $(C-H)_{sp3}$, 1631 (C═N), 1468 ($C═C_{ar}$), 1245, 1153, 1027, 634 and 516 (CF_3SO_3). ^{1}H NMR (CD_2Cl_2, 200 MHz, 300 K) δ, ppm: 8.61 (s, 1H, Ar**H**), 8.48 (s, 2H, N═C**H**), 7.74 (s, 2H, Ar**H**), 4.03 (s broad, 4H, HC═N−C**H**$_2$), 3.34−2.57 (m, 12H, N−C**H**$_2$−C), 2.27 (s broad, 12H, N−C**H**$_3$), 2.05−1.69 (m, 8H, C−C**H**$_2$−C), 1.43 (s, 9H, C−(C**H**$_3$)$_3$).

$[Cu^I_2(^{tBu}L)](ClO_4)_2$, 2ClO$_4$. (>99% Yield.) Anal. Calcd for $C_{28}H_{52}Cl_2Cu_2N_6O_8 \cdot H_2O$ (MW = 798.75 g·mol^{-1}): N, 10.29; C, 41.17; H, 6.66%. Found: N, 10.66; C, 41.29; H, 7.04%. FT-IR (ATR) ν, cm^{-1}: 3271 (N−H), 2929−2865 $(C-H)_{sp3}$, 1627 (C═N), 1468 ($C═C_{ar}$), 1073, 621 (ClO_4). ^{1}H NMR (D_6-acetone, 200 MHz, 300 K) δ, ppm: 8.79 (s, 2H, N═C**H**), 8.66 (s, 1H, Ar**H**), 7.98 (s, 2H, Ar**H**), 4.11 (s broad, 4H, HC═N−C**H**$_2$), 3.25−2.51 (m, 12H, N−C**H**$_2$−C), 2.37 (s broad, 12H, N−C**H**$_3$), 2.03−1.68 (m, 8H, C−C**H**$_2$−C), 1.89 (s, 9H, C−(C**H**$_3$)$_3$). UV−vis (CH_2Cl_2) λ_{max}, nm (ϵ, M^{-1} cm^{-1}): 234 (26 000), 287 (7400).

$[Cu^I_2(^{tBu}L)](SbF_6)_2$, 2SbF$_6$. (67% Yield.) Anal. Calcd for $C_{28}H_{52}Cu_2F_{12}N_6Sb_2 \cdot 1H_2O$ (MW = 1089.36 g·mol^{-1}): N, 7.84; C, 31.39; H, 4.89%. Found: N, 7.71; C, 30.87; H, 5.00%. FT-IR (ATR) ν, cm^{-1}: 2954−2847 $(C-H)_{sp3}$, 1631 (C═N), 1464 ($C═C_{ar}$), 653 (SbF_6). ^{1}H NMR (D_6-acetone, 200 MHz, 300 K) δ, ppm: 8.80 (s, 2H, N═C**H**), 8.74 (s, 1H, Ar**H**), 8.03 (s, 2H, Ar**H**), 4.14 (s broad, 4H, HC═N−C**H**$_2$), 3.30−2.89 (m, 12H, N−C**H**$_2$−C), 2.68 (s broad, 12H, N−C**H**$_3$), 2.00−1.77 (m, 8H, C−C**H**$_2$−C), 1.44 (s, 9H, C−(C**H**$_3$)$_3$).

$[Cu^I_2(^{NO2}L)](CF_3SO_3)_2$, 3CF$_3SO_3$. (85% Yield.) Anal. Calcd for $C_{26}H_{43}Cu_2F_6N_7O_8S_2$ (MW = 886.88 g·mol^{-1}): N, 11.06; C, 35.21; H, 4.89; S, 7.23%. Found: N, 11.40; C, 35.05; H, 5.08; S, 7.14%. FT-IR (ATR) ν, cm^{-1}: 3262 (N−H), 2924−2873 $(C-H)_{sp3}$, 1630 (C═N), 1468 ($C═C_{ar}$), 1538, 1349 (NO_2), 1245, 1154, 1027, 634, 516 (CF_3SO_3). ^{1}H NMR (CD_2Cl_2, 200 MHz, 300 K) δ, ppm: 9.13 (s, 1H, Ar**H**), 8.92 (s, 2H, N═C**H**), 8.55 (s, 2H, Ar**H**), 4.10 (s broad, 4H, HC═N−C**H**$_2$), 3.25−2.66 (m, 12H, N−C**H**$_2$−C), 2.55 (s broad, 12H, N−C**H**$_3$), 1.94−1.75 (m, 8H, C−C**H**$_2$−C).

$[Cu^I_2(^{NO2}L)](ClO_4)_2$, 3ClO$_4$. (97% Yield.) Anal. Calcd for $C_{24}H_{43}Cl_2Cu_2N_7O_{10}$ (MW = 787.64 g·mol^{-1}): N, 12.45; C, 36.60; H, 5.50%. Found: N, 12.22; C, 36.42; H, 6.01%. FT-IR (ATR) ν, cm^{-1}: 3270 (N−H), 2923−2845 $(C-H)_{sp3}$, 1626 (C═N), 1467 ($C═C_{ar}$), 1536, 1347 (NO_2), 1072, 621 (ClO_4). ^{1}H NMR (D_6-acetone, 200 MHz, 300 K) δ, ppm: 9.03 (s, 1H, Ar**H**), 8.99 (s, 2H, N═C**H**), 8.85 (s, 2H, Ar**H**), 4.20 (s broad, 4H, HC═N−C**H**$_2$), 3.45−3.12 (m, 12H, N−C**H**$_2$−C), 2.54 (s broad, 12H, N−C**H**$_3$), 1.65−1.86 (m, 8H, C−C**H**$_2$−C). UV−vis (CH_2Cl_2) λ_{max}, nm (ϵ, M^{-1} cm^{-1}): 229 (47000), 293 (9200), 450 (2900).

$[Cu^I_2(^{NO2}L)](SbF_6)_2$, 3SbF$_6$. (85% Yield.) Anal. Calcd for $C_{24}H_{43}Cu_2F_{12}N_7O_2Sb_2 \cdot {}^1/_3Et_2O$ (MW = 1084.94 g·mol^{-1}): N, 9.04; C, 28.04; H, 4.30%. Found: N, 9.26; C, 27.71; H, 4.66%. FT-IR (ATR) ν, cm^{-1}: 2933 − 2851 $(C-H)_{sp3}$, 1628 (C═N), 1466 ($C═C_{ar}$), 1537, 1347 (NO_2), 652 (SbF_6). ^{1}H NMR (D_6-acetone, 200 MHz, 300 K) δ, ppm: 9.12 (s, 2H, N═C**H**), 8.85−8.82 (m, 3H, Ar**H**), 4.30−4.13 (m, 4H, HC═N−C**H**$_2$), 3.24−2.80 (m, 12H, N−C**H**$_2$−C), 2.59 (s, 12H, N−C**H**$_3$), 1.97−1.84 (m, 8H, C−C**H**$_2$−C).

$[Cu^I_2(^RL)](BArF)_2$ (BArF = $[B\{3,5\text{-}(CF_3)_2C_6H_3\}_4]^-$) were prepared from the corresponding $[Cu_2(^RL)](ClO_4)_2$ complex (R = H, ^{t}Bu, NO_2), as exemplified for **1BArF**.

$[Cu^I_2(^HL)](BArF)_2$, 1BArF. NaBArF (190 mg, 0.21 mmol) was added in small portions directly as a solid to a stirred mixture of **1ClO$_4$** (80 mg, 0.11 mmol) in CH_2Cl_2 (2 mL). The initially insoluble complex quickly dissolved upon NaBArF addition, which caused the formation of a deep orange solution and the appearance of a fine precipitate corresponding to $NaClO_4$. After 2 h under vigorous stirring, the mixture was filtered through Celite and layered with pentane causing the precipitation of the desired compound as an orange solid that was then dried under vacuum (208 mg, 0.09 mmol, 85%). Anal. Calcd for $C_{88}H_{68}B_2Cu_2F_{48}N_6$ (MW = 2270.16 g·

mol^{-1}): N, 3.70 C, 46.56; H, 3.02%. Found: N, 3.81; C, 46.30; H, 3.05%. FT-IR (ATR) ν, cm^{-1}: 2934−2877 (C−H)$_{sp3}$, 1612 (C═N), 1464 (C═C$_{ar}$), 1354, 1271, 1109, 886, 670 (BArF). ^{1}H NMR (D$_6$-acetone, 200 MHz, 300 K) δ, ppm: 8.75 (s, 2H, N═C**H**), 8.58 (d, 2H, J = 7.8 Hz, Ar**H**), 8.39 (s, 1H, Ar**H**), 7.99 (t, 1H, J = 7.8 Hz, Ar**H**), 7.83 (s, 16H, BArF), 7.71 (s, 8H, BarF), 4.32−4.10 (m, 4H, HC═N−C**H**$_2$), 3.31−2.80 (m, 12H, N−**C**H$_2$−C), 2.66 (s broad, 12H, N−C**H**$_3$), 2.00−1.72 (m, 8H, C−C**H**$_2$−C).

[Cu$^{I}_2$(^{tBu}L)](BArF)$_2$, 2BArF. (83% Yield.) Anal. Calcd for $C_{92}H_{76}B_2Cu_2F_{48}N_6$ (MW = 2326.27 g·mol^{-1}): N, 3.61 C, 47.50; H, 3.29%. Found: N, 3.73; C, 47.11; H, 3.20%. FT-IR (ATR) ν, cm^{-1}: 2970−2874 (C−H)$_{sp3}$, 1611 (C═N), 1466 (C═C$_{ar}$), 1354, 1273, 1112, 886, 670 (BArF). ^{1}H NMR (D$_6$-acetone, 200 MHz, 300 K) δ, ppm: 8.83 (m, 3H, N═C**H** + Ar**H**), 8.07 (s, 2H, Ar**H**), 7.82 (s, 16H, BArF), 7.70 (s, 8H, BarF), 4.17 (s broad, 4H, HC═N−C**H**$_2$), 3.32−2.83 (m, 12H, N−**C**H$_2$−C), 2.58 (s, 12H, N−C**H**$_3$), 1.97−1.77 (m, 8H, C−C**H**$_2$−C), 1.44 (s, 9H, C−(C**H**$_3$)$_3$).

[Cu$^{I}_2$(^{NO2}L)](BArF)$_2$, 3BArF. (89% Yield.) Anal. Calcd for $C_{88}H_{67}B_2Cu_2F_{48}N_7O_2$ (MW = 2315.16 g·mol^{-1}): N, 4.24; C, 45.65; H, 2.42%. Found: N, 4.09; C, 45.50; H, 3.05%. FT-IR (ATR) ν, cm^{-1}: 2947−2884 (C−H)$_{sp3}$, 1611 (C═N), 1549 (NO$_2$), 1465 (C═C$_{ar}$), 1354, 1272, 1112, 886, 670 (BArF). ^{1}H NMR (D$_6$-acetone, 200 MHz, 300 K) δ, ppm: 9.22 (s, 2H, N═C**H**), 8.89 (s, 2H, Ar**H**), 8.83 (s, 1H, Ar**H**), 7.82 (s, 16H, BArF), 7.70 (s, 8H, BArF), 4.38−4.19 (m, 4H, HC═N−C**H**$_2$), 3.27−2.86 (m, 12H, N−C**H**$_2$−C), 2.60 (s, 12H, N−C**H**$_3$), 2.00−1.81 (m, 8H, C−C**H**$_2$−C).

Oxygenation Reactions. Analysis of the ligand after oxygenation reactions at low temperature was done as exemplified for **1ClO$_4$**. In an anaerobic box, **1ClO$_4$** (96 mg, 0.13 mmol) was loaded in a Schlenk flask equipped with a stirring bar, capped with a rubber septum, and taken out of the box. Previously deoxygenated dry acetone (85 mL) was added via a cannula at room-temperature generating a clear deep orange solution. The solution was cooled down to −90 °C by immersion in a liquid N_2/methanol bath, and O_2 was then allowed into the reaction vessel via a needle connected to a dry O_2-filled balloon, causing the solution to change from orange to deep yellow. The solution was stirred at −90 °C for an hour, slowly turning to green, and then it was slowly warmed up to room temperature. Volatiles were removed under vacuum, and the remaining oily residue was treated with 6 M HCl (2 mL). The mixture was stirred for 15 min, and then it was extracted with CH_2Cl_2 (3 × 10 mL). The combined organic fractions were dried over $MgSO_4$, and the solvent was removed under vacuum to obtain a crystalline pale yellow solid, which was spectroscopically analyzed as benzene-1,3-dialdehyde (6.4 mg, 0.048 mmol, 37%). ^{1}H NMR (200 MHz, $CDCl_3$, 300K) δ, ppm: 10.16 (s, 2H), 8.42 (d, J = 2 Hz, 1H), 8.19 (dd, 2H, J_1 = 8 Hz, J_2 = 2 Hz), 7.77 (t, 2H, J = 8 Hz).

Attempts to extract the amine residues from the aqueous phase after basic workup afforded oily residues with ^{1}H NMR spectra showing broad features that could not be interpreted. GC-MS analysis was also unsuccessful.

Analysis after low-temperature oxidation of **2ClO$_4$**. There was a 7.9 mg (44%) yield of 5-*tert*-butylbenzene-1,3-dicarbaldehyde. ^{1}H NMR (200 MHz, $CDCl_3$, 300 K) δ, ppm: 10.14 (s, 2H, C**H**O), 8.22 (s, 3H, Ar**H**), 1.44 (s, 9H, C−(C**H**$_3$)$_3$).

Analysis after low-temperature oxidation of **3ClO$_4$**. There was a 21.8 mg (98%) yield of 5-nitro-benzene-1,3-dicarbaldehyde. ^{1}H NMR (200 MHz, $CDCl_3$, 300 K) δ, ppm: 10.21 (s, 2H, C**H**O), 8.96 (s, 2H, Ar**H**), 8.72 (s, 1H, Ar**H**).

Kinetic Measurements. The kinetic measurements were performed using a Hi-Tech Scientific (presently, TgK Scientific, Salisbury, Wiltshire, U.K.) SF-43 cryogenic double-mixing stopped-flow instrument equipped with stainless steel plumbing, a 1.00 cm stainless steel mixing cell with sapphire windows, and an anaerobic gas-flushing kit. The instrument was connected to an IBM computer with IS-2 Rapid Kinetics Software by Hi-Tech Scientific (presently TgK Scientific). The mixing cell was maintained to ± 0.1 K, and the mixing time was 2−3 ms. The source of light was either a visible lamp combined with a monochromator (low-intensity light irradiation of the sample) or a xenon lamp combined with a diode array rapid scanning unit (strong UV−vis irradiation of the sample). All manipulations with the copper complexes and their solutions were done using an argon atmosphere glovebox, gas-tight syringes, and the anaerobic stopped-flow instrument to avoid contamination with air. Saturated solutions of O_2 in acetone were prepared by bubbling the dry O_2 gas for 10 min in a septum-closed gas-tight syringes with the solvent at a constant temperature (25 °C). The solubility of O_2 was accepted to be 8.0 mM in acetone at 25 °C. Solutions with lower O_2 concentrations were prepared by dilution of a saturated solution of oxygen with the corresponding amount of solvent containing no dissolved oxygen in gastight syringes. The solutions of dicopper(I) complex and O_2 were cooled to a preset temperature in the stopped-flow instrument before mixing. The concentrations of the reactants were corrected for the 1:1 mixing ratio.

For all the kinetic experiments, dioxygen was always taken in large excess so that its concentration did not change significantly during the reaction with the dicopper(I) complex.

For the oxygenation reactions in acetone, the kinetic traces obtained under the pseudo-first-order conditions over 3−5 half-lives were fitted globally with Specfit32 software (Bio-Logic, Claix, France) or at single wavelengths with IS-2 Rapid Scanning Kinetic Software to eq 1.

$$A_t = A_\infty - (A_\infty - A_0)\cdot\exp(-k_{obs}t) \quad (1)$$

Equation 2 was used to calculate the second-order rate constant k.

$$k = k_{obs}/[O_2] \quad (2)$$

$$-\frac{d[LCu_2]}{dt} = k_{obs}[LCu_2] = k[O_2][LCu_2] \quad (3)$$

The fit of the experimental data to eq 1 and the independence of k_{obs} on [LCu$^{I}_2$] served as a proof of the first-order behavior of the reactions in the dicopper(I) complex. A linear dependence of k_{obs} on [O_2] served as proof of the first-order behavior of the reactions in dioxygen.

The values of k (M^{-1} s^{-1}) were determined at different temperatures and fitted to the Eyring equation, eq 4, to obtain the activation parameters $\Delta H^{\ddagger}$ and $\Delta S^{\ddagger}$. See more discussion elsewhere in the paper about determination of the activation parameters.

$$\ln(k/T) = 23.76 + \Delta S^{\ddagger}/R - \Delta H^{\ddagger}/RT \quad (4)$$

Physical Methods. IR spectra were taken in a Mattson-Galaxy Satellite FT-IR spectrophotometer using a MKII Golden Gate single reflection ATR system. UV−vis spectroscopy was performed on a Cary 50 Scan (Varian) UV−vis spectrophotometer with 1 cm quartz cells or with an immersion probe of 5 mm path length. Cyclic voltammetric (CV) experiments were performed in an IJ-Cambria IH-660 potentiostat using a three electrode cell. Glassy carbon disk electrodes (3 mm diameter) from BAS were used as working electrode, platinum wire was used as auxiliary, and SSCE was used as the reference electrode (all the potentials given in this work are always with regard to this reference electrode). Unless explicitly

mentioned, all cyclic voltammograms presented in this work were recorded at 100 mV/s scan rate under nitrogen atmosphere. The complexes were dissolved in previously degassed solvents containing the necessary amount of n-Bu_4NPF_6 (TBAH) as supporting electrolyte to yield a 0.1 M ionic strength solution. All $E_{1/2}$ values reported in this work were estimated from cyclic voltammetric experiments as the average of the oxidative and reductive peak potentials ($E_{pa} + E_{pc}$)/2. NMR spectra were taken on Bruker DPX200, Bruker DPX250, Bruker DPX360, and Bruker DRX500 spectrometers. One- and two-dimensional NMR experiments were recorded using standard conditions. All 2D NOESY experiments were collected using a mixing time of 500 ms. Variable temperature (VT) NMR experiments were recorded when necessary to identify NOEs and chemical exchange cross-peaks. ^{1}H NMR spectra were referenced to the residual solvents peaks or TMS (tetramethylsilane). ^{19}F NMR spectra were referenced to CCl_3F. Elemental analyses were performed using a CHNS-O EA-1108 elemental analyzer from Fisons. The ESI-MS experiments were performed on a Navigator LC/MS chromatograph from Thermo Quest Finnigan, using methanol or acetonitrile as a mobile phase.

Resonance Raman spectra were collected on an Acton AM-506 spectrometer (1200 groove grating) using a Kaiser Optical holographic super-notch filter with a Princeton Instruments liquid-N_2-cooled (LN-1100PB) CCD detector with a 4 cm^{-1} spectral resolution. The 407 cm^{-1} laser excitation line was obtained with a Spectra Physics BeamLok 2060-KR-V krypton ion laser. The Raman frequencies were referenced to indene. The spectra were obtained from samples prepared in a glovebox, that after exposition to pure O_2 were frozen at 77 K using a gold-plated copper cold finger in thermal contact with a Dewar containing liquid N_2. The power recorded at the laser for each sample was 120 mW. No photobleaching was observed upon repeated scans. Curve fits (Gaussian functions) and baseline corrections (polynomial fits) were carried out using Grams/32 Spectral Notebase Version 4.04 (Galactic).

Crystal Data Collection, Structure Solution, and Refinement Details for Compounds $1ClO_4$ and $2CF_3SO_3$. Crystal structure determination for $\mathbf{1ClO_4}$ was carried out using a Siemens *P*4 diffractometer equipped with a SMART-CCD-1000 area detector, a MACScience Co rotating anode with Mo K radiation, a graphite monochromator, and a Siemens low-temperature device LT2 ($T = -120$ °C). Full-sphere data collection using ω and φ scans was performed. The programs that were used follow: data collection Smart V. 5.060 (BrukerAXS 1999), data reduction Saint + Version 6.02 (Bruker AXS 1999), and absorption correction SADABS (Bruker AXS 1999). Crystal structure solution was achieved using direct methods as implemented in SHELXTL Version 5.10 (Sheldrick, Universtität Göttingen (Germany), 1998) and visualized using XP program. Crystals of $\mathbf{2CF_3SO_3}$ were mounted on a nylon loop and used for low temperature (100(2) K) X-ray structure determination. The measurements were carried out on a Bruker Smart Apex CCD diffractometer using graphite-monochromated Mo Kα radiation ($\lambda = 0.71073$ Å). The measurements were made in the range 2.03−28.36° for θ. Full-sphere data collection was carried out with ω and φ scans. For $\mathbf{2CF_3SO_3}$, a total of 59908 reflections were collected of which 9604 [R(int) = 0.0472] were unique. The programs that were used follow: data collection Smart version 5.625 (Bruker AXS 1997−01); data reduction Saint + version 6.36A (Bruker AXS 2001); absorption correction SADABS version 2.05 (Bruker AXS 2001). Crystal structure solution was achieved using direct methods as implemented in SHELXTL Version 6.12 (Bruker AXS 2001) and visualized using XP program. The structure was solved by direct methods and refined by full-matrix least-squares methods on F^2. Non-hydrogen atoms were refined anisotropically. The hydrogen atoms were placed in geometrically optimized positions and forced to ride on the atoms to which they are attached, except those attached to nitrogen, which were placed from the electron density difference map.

Table 1 summarizes the crystallographic refinement parameters for complexes $\mathbf{1ClO_4}$ and $\mathbf{2CF_3SO_3}$, and selected bond lengths (Å) and angles (deg) are collected in Table 2.

Crystallographic refinement parameters for $\mathbf{2ClO_4}$ and $\mathbf{3BArF\cdot CH_3CN}$, and a list of selected bond lengths (Å) and angles (deg), are collected as Supporting Information.

Computational Details. All geometry optimizations have been performed at the B3LYP level,[21−23] using the standard 6-31G* basis set[24] with the Gaussian03 package.[25] The geometry optimizations were performed without symmetry constraints, and the nature of extrema was checked by analytical frequency calculations. The energies discussed throughout the text include ZPE corrections.

Results and Discussion

Ligand and Complex Synthesis. Hexaaza podand ligands ^{R}L, R = H, ^{t}Bu, and NO_2 (Scheme 2), were chosen as dinucleating ligand scaffolds because they possess two potential metal binding sites, each of which consist of three N atoms that constitute the most common coordination environment for protein copper sites involved in O_2 binding and activation.[2] In addition, this family of ligands is structurally related to the macrocyclic ligand sb3m, previously described by Martell et al. (Scheme 1),[10,16] albeit lacking the structural constraints imposed by the macrocyclic frame. Electron donating (^{t}Bu) and withdrawing groups (NO_2) were introduced in the aromatic ring with the aim of fine-tuning the basicity properties of the imine N atoms and affecting the electronic properties of the copper ions. ^{R}L, R = H, ^{t}Bu, or NO_2, were prepared by condensation of a benzene-1,3-dialdehyde with the corresponding dialkyl capped triamine (Scheme 2). The ^{1}H NMR spectra of the ligands exhibit complicated patterns that could be best understood on the basis of the nucleophilic attack of the amine group over the imine, as already described in related hexaazamacrocyclic ligands.[12]

Reaction in acetonitrile of each ligand with 2 equiv of $[Cu^I(CH_3CN)_4]X$ (X = CF_3SO_3, ClO_4, or SbF_6, Scheme 2)

(21) Becke, A. D. *J. Chem. Phys.* **1993**, *98*, 5648−5652.
(22) Lee, C.; Yang, W.; Parr, R. G. *Phys. Rev. B* **1988**, *37*, 785−789.
(23) Stevens, P. J.; Devlin, F. J.; Chabalowski, C. F.; Frisch, M. J. *J. Phys. Chem.* **1994**, *98*, 11623−11627.
(24) Hehre, W. J.; Radom, L.; Schleyer, P. V. R.; Pople, J. A. *Ab Initio Molecular Orbital Theory*; Wiley: New York, 1986.
(25) Frisch, M. J.; Trucks, G. W.; Schlegel, H. B.; Scuseria, G. E.; Robb, M. A.; Cheeseman, J. R.; Montgomery, J. A., Jr.; Vreven, T.; Kudin, K. N.; Burant, J. C.; Millam, J. M.; Iyengar, S. S.; Tomasi, J.; Barone, V.; Mennucci, B.; Cossi, M.; Scalmani, G.; Rega, N.; Petersson, G. A.; Nakatsuji, H.; Hada, M.; Ehara, M.; Toyota, K.; Fukuda, R.; Hasegawa, J.; Ishida, M.; Nakajima, T.; Honda, Y.; Kitao, O.; Nakai, H.; Klene, M.; Li, X.; Knox, J. E.; Hratchian, H. P.; Cross, J. B.; Bakken, V.; Adamo, C.; Jaramillo, J.; Gomperts, R.; Stratmann, R. E.; Yazyev, O.; Austin, A. J.; Cammi, R.; Pomelli, C.; Ochterski, J. W.; Ayala, P. Y.; Morokuma, K.; Voth, G. A.; Salvador, P.; Dannenberg, J. J.; Zakrzewski, V. G.; Dapprich, S.; Daniels, A. D.; Strain, M. C.; Farkas, O.; Malick, D. K.; Rabuck, A. D.; Raghavachari, K.; Foresman, J. B.; Ortiz, J. V.; Cui, Q.; Baboul, A. G.; Clifford, S.; Cioslowski, J.; Stefanov, B. B.; Liu, G.; Liashenko, A.; Piskorz, P.; Komaromi, I.; Martin, R. L.; Fox, D. J.; Keith, T.; Al-Laham, M. A.; Peng, C. Y.; Nanayakkara, A.; Challacombe, M.; Gill, P. M. W.; Johnson, B.; Chen, W.; Wong, M. W.; Gonzalez, C.; Pople, J. A. *Gaussian 03*, revision C.02; Gaussian, Inc.: Wallingford, CT, 2004.

Table 1. Crystal Data and Structure Refinement Parameters for **1ClO$_4$** and **2CF$_3$SO$_3$**

	1ClO$_4$	**2CF$_3$SO$_3$**
empirical formula	$C_{28}H_{50}Cl_2Cu_2N_8O_8$	$C_{30}H_{51}Cu_2F_6N_6O_6S_2$
fw	824.74	896.97
T	153(2) K	100(2) K
wavelength	0.71073 Å	0.71073 Å
cryst syst	triclinic	monoclinic
space group	$P\bar{1}$	$P2_1/c$
unit cell dimensions	$a = 9.5895(3)$ Å	$a = 16.0444(16)$ Å
	$\alpha = 106.4670(10)°$	$\alpha = 90°$
	$b = 13.2032(5)$ Å	$b = 14.7659(14)$ Å
	$\beta = 98.7860(10)°$	$\beta = 102.048(6)°$
	$c = 15.7764(6)$ Å	$c = 17.4280(17)$ Å
	$\gamma = 94.5510(10)°$	$\gamma = 90°$
V	1877.16(12) Å^3	3878.1(7) Å^3
Z	2	4
density (calcd)	1.459 Mg·m^{-3}	1.536 Mg·m^{-3}
abs coeff	1.330 mm^{-1}	1.281 mm^{-1}
F(000)	860	1860
cryst size (mm^3)	0.3 × 0.6 × 0.6	0.5 × 0.2 × 0.2
Θ range for data collection	1.62−31.43°	2.03−28.36°
index ranges	$-13 \le h \le 13$	$-21 \le h \le 21$
	$-18 \le k \le 18$	$-19 \le k \le 19$
	$-22 \le l \le 22$	$-22 \le l \le 22$
reflns collected	29209	59908
indep reflns	11550 [R(int) = 0.0593]	9604 [R(int) = 0.0472]
completeness to Θ	31.43° 93.1%	28.36° 98.8%
refinement method	full-matrix least-squares on F^2	full-matrix least-squares on F^2
data/restraints/params	11550/3/475	9604/0/484
GOF on F^2	0.949	1.062
final *R* indices [$I > 2\sigma(I)$] R1, wR2	R1 = 0.0400	R1 = 0.0328
	wR2 = 0.0982	wR2 = 0.0853
R indices (all data) R1, wR2	R1 = 0.0582	R1 = 0.0423
	wR2 = 0.1048	wR2 = 0.0887
largest diff peak and hole	0.655 and −0.771 e Å^{-3}	0.892 and −0.721 e Å^{-3}

Table 2. Selected Bond Lengths [Å] and Angles [deg] for **1ClO$_4$** and **2CF$_3$SO$_3$**

1ClO$_4$		**2CF$_3$SO$_3$**	
Cu(1)N(3)	1.9174(15)	Cu(1)N(4)	1.9284(15)
Cu(1)N(2)	1.9787(15)	Cu(1)N(6)	1.9866(16)
Cu(1)N(1)	2.1392(16)	Cu(1)N(5)	2.1261(16)
Cu(2)N(4)	1.9272(15)	Cu(2)N(1)	2.0208(16)
Cu(2)N(5)	1.9970(16)	Cu(2)O(1)	2.3526(16)
Cu(2)N(6)	2.1198(16)	Cu(2)N(3)	1.9483(16)
N(3)Cu(1)N(2)	154.04(6)	Cu(2)N(2)	2.1224(16)
N(3)Cu(1)N(1)	107.01(6)	N(4)Cu(1)N(6)	155.58(6)
N(2)Cu(1)N(1)	98.92(6)	N(4)Cu(1)N(5)	103.16(6)
N(4)Cu(2)N(5)	146.62(6)	N(6)Cu(1)N(5)	101.18(6)
N(4)Cu(2)N(6)	111.40(6)	N(3)Cu(2)N(1)	153.37(6)
N(5)Cu(2)N(6)	101.90(6)	N(3)Cu(2)N(2)	99.11(6)
		N(1)Cu(2) N(2)	100.91(7)
		N(3)Cu(2)O(1)	97.31(6)
		N(1)Cu(2)O(1)	98.11(6)
		N(2)Cu(2)O(1)	95.36(6)

under rigorously anaerobic conditions resulted in dark orange solutions from which the binuclear complexes $[Cu^I_2(^RL)](X)_2$ (R = H, **1X**; R = ^{t}Bu, **2X**; and R = NO_2, **3X**) could be isolated in good yields (74−99%) by precipitation induced by diethyl ether addition. $[Cu^I_2(^RL)](BArF)_2$ complexes (**1BArF**−**3BArF**) were obtained by reaction of the corresponding perchlorate complexes with 2 equiv of NaBArF in CH_2Cl_2 and isolated by the addition of pentane. The compounds were further purified by recrystallization from slow diethyl ether diffusion over acetonitrile solutions of the complexes. The Cu^I ions in these complexes (even those isolated from acetonitrile) are three-coordinated in the solid state, as ascertained by combustion analysis, ^{1}H NMR, and, with the single exception of **3BArF·CH$_3$CN**, X-ray crystallography (vide infra). Orange X-ray quality crystals could be obtained for **1ClO$_4$**, **2ClO$_4$**, **2CF$_3$SO$_3$**, and **3BArF·CH$_3$CN**. Crystals of **3BArF·CH$_3$CN** were of marginal quality, and they allowed us to obtain reliable connectivity and identity information but not accurate metrical parameters.

Solid-State Structures. Experimental details of the crystal structure determination of complexes **1ClO$_4$** and **2CF$_3$SO$_3$** are collected in Table 1, and a list of selected bond distances and angles can be found in Table 2. ORTEP diagrams of the cationic parts of **1ClO$_4$** and **2CF$_3$SO$_3$** are shown in Figure 1. Experimental details, a list of selected bond distances and angles, and ORTEP diagrams for the cationic parts of **2ClO$_4$** and **3BArF·CH$_3$CN** are provided as Supporting Information.

The crystallographic unit in **1ClO$_4$** is composed of a binuclear copper complex, two perchlorate anions, and two acetonitrile molecules (Figure 1). Each ligand unit is ligated to four different copper ions, one for each of the two imine groups and the other two chelated by the two amine groups of each ligand arm. Each of the two triamine ligand arms runs along a triamine arm from a second molecule, with two copper atoms bound between them. Each copper ion is three-coordinated, i.e., bound to two amine N atoms from a ligand unit and a third imine N atom from a second ligand molecule. This results in a polymeric chain structure shown in Figure 1. The structure is completed with two perchlorate counterions and two noninteracting acetonitrile molecules. The coordination environment of each copper ion is distorted trigonal planar, but the N−Cu−N angles suffer severe

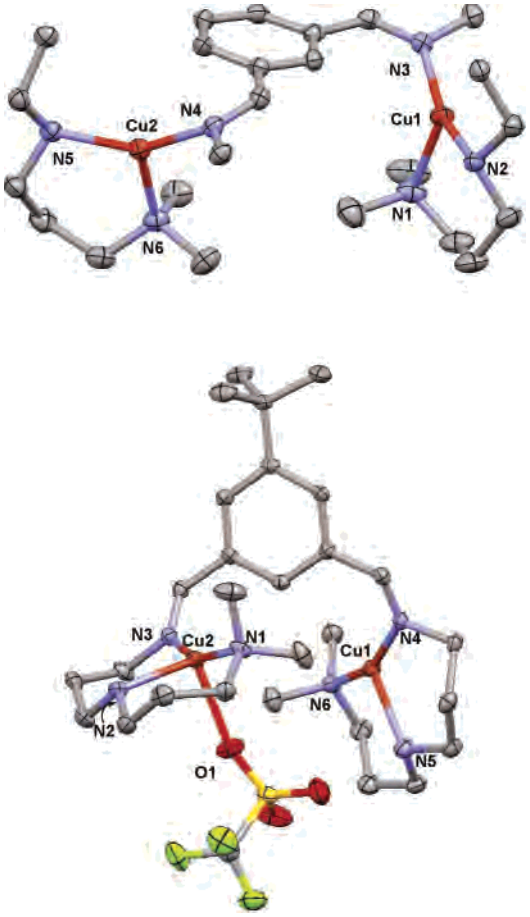

Figure 1. ORTEP diagram (50%) of the crystallographic unit of the polymeric cationic chain $\{[Cu^{I}_2(^{H}L)](ClO_4)_2\}_n$, **1ClO$_4$** (top), and the cationic part of $[Cu^{I}_2(^{tBu}L)](CF_3SO_3)_2$, **2CF$_3SO_3$** (bottom). H atoms and solvent molecules have been omitted for clarity.

distortions from the theoretical 120°; thus, the six-membered chelate ring imposes a rather acute ~100° for the $N_{ter}-Cu-N_{sec}$ angle, and the $N_{im}-Cu-N_{sec}$ angle appears to open up to ~150°, likely reflecting structural strains arising from the relative spatial arrangement of two different ligand units. The average Cu−N imine distance is 1.922 Å and it is significantly shorter than the $Cu-N_{ter}$ (tertiary amines, 2.129 Å) and $Cu-N_{sec}$ (secondary amines, 1.987 Å) values. All of them are within the range of distances described in the literature for related complexes.[9,10,26−35]

2ClO$_4$, **2CF$_3$SO$_3$**, and **3BArF·CH$_3$CN** present a monomeric structure, and the main structural characteristics of the coordination environment of the copper ion in **2ClO$_4$** and **2CF$_3$SO$_3$** are similar. The solid-state structures of **2ClO$_4$** and **2CF$_3$SO$_3$** consist of a cationic binuclear copper complex, where one of the Cu ions is bound to a perchlorate/triflate anion, and a second noninteracting counterion balances the charge. Because of the similarity between the structures of **2ClO$_4$** and **2CF$_3$SO$_3$**, only the latter will be discussed, and details of the crystallographic analysis of the former are reported in the Supporting Information. The coordination geometry of the three coordinated copper atom is between T-shape and distorted trigonal planar (Figure 1), with two acute N−Cu−N angles (99.11(6)−103.16(6)°) for the six-membered chelate rings, which in turn also causes the opening of the third N−Cu−N angle (153.37(6)−155.58(6)°). Each of the six-membered chelate rings adopts chairlike conformations. The N_3Cu unit corresponding to the second copper ion shares similar metrical parameters, but its coordination environment is now completed by an O atom from a triflate anion at a relatively long distance (2.3526(16) Å), with the Cu−O vector being nearly perpendicular to the nearly coplanar N_3Cu unit (N(2)Cu(2)O(1) angle is 95.36(6)°). The three Cu−N distances of both copper ions also parallel those exhibited by **1ClO$_4$**; the shortest Cu−N distance corresponds to the imine N atom (1.9284(15)−1.9483(16) Å), and the longest is observed for the $Cu-N_{sec}$ bond (2.1261(16)−2.1224(16) Å). Overall, the relative order in the Cu−N distances could be understood on the basis of the higher preference of the soft Cu^{I} ion for the soft imine group rather than for the hard amine. Finally, the least-squares fitted planes defined by the two N_3Cu units are nearly perpendicular (79.52°). The crystal structure of **3BArF·CH$_3$CN**, shown as Supporting Information, contains a dinuclear copper complex, and two BArF counterions balance the charge. One of the copper ions is three-coordinate, and its coordination geometry resembles the one described for **2X** (X = ClO_4 and CF_3SO_3). On the other hand, the second copper ion is tetracoordinate; three coordination positions are occupied by the three N atoms of the ligand, and the fourth site of the distorted tetrahedron is filled with an acetonitrile molecule. Nevertheless, the acetonitrile molecule is readily lost upon drying under vacuum, as evidenced by ^{1}H NMR and combustion analysis. The poor quality of the crystals precludes discussion of the metric parameters.

Comparison between the solid-state structures of **2X** (X = ClO_4, CF_3SO_3) and macrocyclic $[Cu^{I}_2(sb3m)](ClO_4)_2$ (Scheme 1) reveals structural similarities; the coordination geometries for the copper ions are all between T-shaped and trigonal planar,[10] although for $[Cu^{I}_2(sb3m)](ClO_4)_2$ each copper ion has a weak interaction with a perchlorate anion (Cu−O distance is 2.935(3) Å). Furthermore, $Cu-N_{im}$ (~1.94 Å) and $Cu-N_{sec}$ (~2.11 Å) distances are also comparable. The main difference between the three structures is the relative orientation of the N_3Cu sets, nearly parallel for the macrocyclic structure and almost perpendicular for

(26) Nelson, S. M.; Esho, F.; Lavery, A.; Drew, M. G. B. *J. Am. Chem. Soc.* **1983**, *105*, 5693−5695.
(27) Gelling, O. J.; van Bolhuis, F.; Meetsma, A.; Feringa, B. L. *J. Chem. Soc., Chem. Commun.* **1988**, 552−554.
(28) Comba, P.; Hambley, T. W.; Hilfenhaus, P.; Richens, D. T. *J. Chem. Soc., Dalton Trans.* **1996**, *4*, 533−539.
(29) Pasquali, M.; Floriani, C.; Gaetani-Manfredotti, A.; Villa, A. C. *Inorg. Chem.* **1979**, *18*, 3535−3542.
(30) Scott, M. J.; Holm, R. H. *J. Am. Chem. Soc.* **1994**, *116*, 11357−11367.
(31) Hubin, T. J.; Alcock, N. W.; Busch, D. H. *Acta Crystallogr., Sect. C* **2000**, *56*, 37−39.
(32) Becker, M.; Heinemann, F. W.; Knoch, F.; Donaubauer, W.; Liehr, G.; Schindler, S.; Golub, G.; Cohen, H.; Meyerstein, D. *Eur. J. Inorg. Chem.* **2000**, *4*, 719−726.
(33) Liang, H.-C.; Zhang, C. X.; Henson, M. J.; Sommer, R. D.; Hatwell, K. R.; Kaderli, S.; Zuberbühler, A. D.; Rheingold, A. L.; Solomon, E. I.; Karlin, K. D. *J. Am. Chem. Soc.* **2002**, *124*, 4170−4171.
(34) Costas, M.; Xifra, R.; Llobet, A.; Solà, M.; Robles, J.; Parella, T.; Stoeckli-Evans, H.; Neuburger, M. *Inorg. Chem.* **2003**, *42*, 4456−4468.
(35) Cole, A. P.; Mahadevan, V.; Mirica, L. M.; Ottenwaelder, X.; Stack, T. D. P. *Inorg. Chem.* **2006**, *44*, 7345−7364.

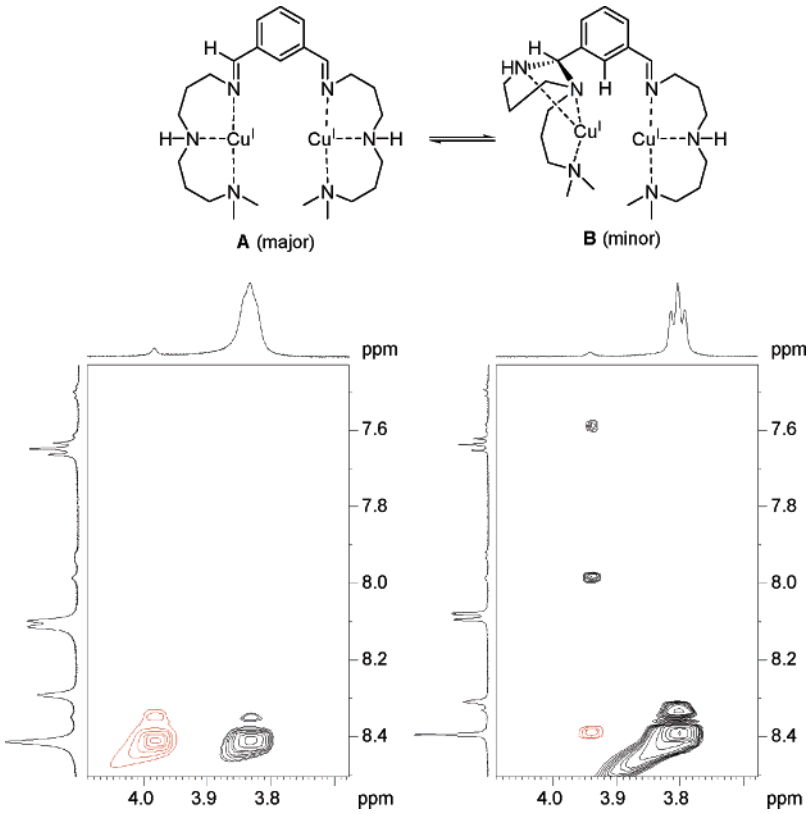

Figure 2. $^1H-^1H$ NOESY spectra of **1ClO$_4$** in CD_3CN recorded at 298 K (bottom left) and 240 K (bottom right) and the isomerically related forms of the copper complex in solution (top). Negative exchange cross-peaks are marked in red whereas NOE cross-peaks are marked in black.

the podand analogue. The Cu···Cu distance is also significantly different, ~5.1 Å for **2X** (X = ClO_4, CF_3SO_3), but up to 7.7 Å for the macrocycle. Interestingly, the Cu···Cu distance in **3BArF·CH$_3$CN** is even larger (~8.4 Å).

Solution Structure: NMR Spectroscopy. The structure of the complexes in solution was studied by NMR spectroscopy. Despite the different solid-state structures ascertained by crystallography, **1X**−**3X** (X = CF_3SO_3, ClO_4, SbF_6, and BArF) complexes exhibit similar ^1H NMR spectra, suggesting that analogous species are present in solution. The somewhat different solid-state structures exhibited by these dynamic complexes (vide infra) are therefore most likely due to packing effects on the solid state that displace the equilibrium toward a thermodynamically preferred solid-state structure. Owing to the similarity of the spectra, only **1X** (X = ClO_4, SbF_6, CF_3SO_3, BArF) was studied in detail. The room temperature ^1H NMR spectrum of **1ClO$_4$** in CD_3CN is characterized by broad signals that sharpen upon lowering the temperature, suggesting a fluxional behavior (Figure S1). Such dynamic behavior has been previously documented in related macrocyclic complexes and may be ascribed to the low charge and the lack of crystal field stabilization energy for the d^{10} Cu^I ion, which give rise to relatively weak Cu−N bonds.[10,34]

The aromatic region of the spectrum contains two sets of signals **A**:**B** in a 5:1 relative ratio, and magnetization transfer experiments indicate that both species undergo an exchange process that is practically frozen at −40 °C. Pulse gradient spin−echo (PGSE) measurements of **1ClO$_4$** in CD_3CN at 292 K afford the same diffusion coefficient value ($k = -8.57 \times 10^{-10}$ m^2/s) for both species. This strongly suggests that the structures of the two components of **1ClO$_4$** in solution are monomeric in nature and that the polymeric structure determined by X-ray crystallography is not retained in solution. Two-dimensional $^1H-^1H$ and $^1H-^{13}C$ COSY correlations have allowed a full assignment of the spectra, and further insights into the structures of the two species in solution could be gained by NOESY correlations (Scheme S1, Figures S2−S6). On the basis of these experiments, the major species is assigned to the bis-imine form **A** (Figure 2), which matches the X-ray determined structure of **2ClO$_4$**, provided dynamic processes allow symmetry equivalence between the two binding domains on the time scale of the ^1H NMR experiment. Acetonitrile binding to the Cu ions may also be possible, as observed in the crystal structure of **3BArF**, but its binding could not be definitively established by NMR.

On the other hand, elucidation of the structure for the minor species **B** (Figure 2) is based in the lack of symmetry between the two binding sites. The presence of a negative exchange (EXSY) cross-peak in the corresponding NOESY spectrum at 298 K between the imine proton of the major conformation **A** (8.41 ppm) and a methine CH proton belonging to the minor conformation **B** (3.98 ppm) confirms the slow equilibrium in the NMR time-scale existing between **A** and **B** forms (Figure 2). This equilibrium is also evidenced for all strong EXSY cross-peaks observed between all signals of the major and the minor conformations at 298 K but that practically disappear at 240 K. The structure characterization of the minor conformation **B** that involves the presence of a

Table 3. Spectroscopic and Electrochemical Properties of the Copper Complexes **1**−**3X**, and Their Corresponding CO-Adducts

complex	UV−vis λ_{max}, nm (ϵ, M^{-1} cm^{-1})[a]	E_{pa}/E_{pc},[b] mV	FT-IR ν_{st} CO,[c] cm^{-1}
1X	412 (1700)	878/−405	2085
2X	412 (1500)	861/−332	2085
3X	450 (2900)	811/−392	2089

[a] X = ClO_4. [b] X = SbF_6. [c] X = CF_3SO_3.

1,3-diaminecyclohexyl ring was also performed thanks to two-dimensional NMR techniques at different temperatures (Figures S3−S6). Full spectral assignment is summarized in Scheme S1. Again, acetonitrile binding to the Cu ion is possible, but could not be definitively proven.

Despite the existence of the described equilibrium between **A** and **B** in CD_3CN, this process has not been observed in other solvents. The use of CD_2Cl_2 or D_6-acetone gives rise to simpler ^1H NMR spectra with only one set of signals in the aromatic region indicative of only one type of species corresponding to **A**, where the two binding sites are symmetrically related on the NMR time scale (Figures S7−S8). A possible explanation for the solvent dependent spectra is the different coordination properties of the three solvents. Acetonitrile is the most coordinating solvent, and it can easily interact with the metal center causing an elongation of the Cu−N distances and thus allowing the isomerization of the ligand and the formation of the **B** isomer. On the other hand, acetone and dichloromethane do not interact as strongly with the copper(I) center, so the amine ligands remain more tightly bound and they are prevented from attacking the imine. VT (variable temperature) spectra of **1CF$_3$SO$_3$** in CD_2Cl_2 and D_6-acetone reveal partial resolution of the initially broad features of the spectra, but the signals do not completely resolve even at 213 K. These observations again suggest a fluxional behavior of the complexes in solution. PGSE measurements of **1CF$_3$SO$_3$** afford diffusion coefficient values (-6.0×10^{-10} m^2/s in D_6-acetone at 240 K) consistent with a monomeric nature of the species in solution (Figure S9).

Finally, ^{19}F NMR spectra referenced to CCl_3F of **1CF$_3$SO$_3$** in CD_2Cl_2 and D_6-acetone (Figure S10) at 298 K exhibit a relatively broad ($\Delta\delta_{1/2}$ = 562 and 435 Hz, respectively) single resonance at $\delta = -78.0$ and -78.2 ppm, respectively, that downshifts ($\delta = -79.3$ and -79.2 ppm) and significantly sharpens ($\Delta\delta_{1/2}$ = 312 and 187 Hz, respectively) at 213 K. We conclude that the CF_3SO_3 group is engaged in some type of dynamic process, faster than the ^{19}F NMR time scale. On the basis of the crystallographic analysis, we suggest that this process involves fast and reversible binding of the weakly coordinating triflate group to a copper center, combined with fluxional motions of the complex, as evidenced by ^1H NMR spectroscopy.

UV−Vis Spectroscopy and Cyclic Voltammetry. Solutions of **1**−**3X** complexes in CH_2Cl_2 exhibit orange colors arising from intense bands in their UV−vis spectra at about 430 nm ($\epsilon \sim 3000$ M^{-1} cm^{-1}) (Figure S11, Table 3). On the basis of their high extinction coefficients and the d^{10} electronic configuration of the Cu^I ion, these bands can be interpreted as copper-to-imine charge-transfer transitions. In support of this assignment, the $[Cu^I_2(m\text{-}XYL^{MeAN})]^{2+}$ complex, where the imine group has been reduced, is colorless. The UV−vis spectra of **1ClO$_4$** and **2ClO$_4$** are quite similar, but their extinction coefficients are lower than those of **3ClO$_4$** which can be attributed to the effect of the NO_2 group as was already pointed out for related Cu^I complexes described by Karlin et al.[36]

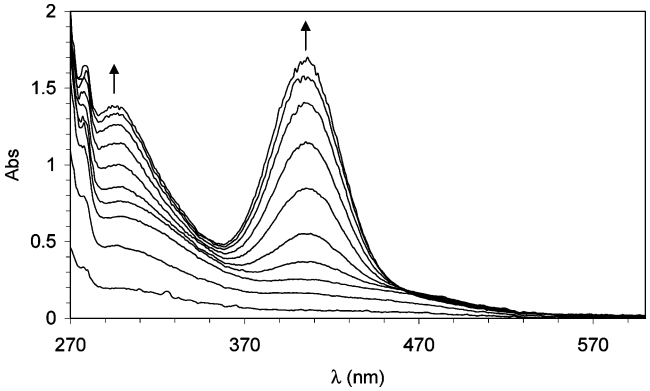

Figure 3. Benchtop recorded UV−vis spectra (183 K) in THF of the reaction of **1BArF** (0.18 mM) with O_2 generating $[Cu^{III}_2(\mu\text{-}O)_2{}^HL]^{2+}$. Spectra are taken every 12 s. (The rate depends on mass transport and differs from the rates of the chemical reaction between Cu(I) and O_2 determined in stopped-flow experiments, see below.)

Cyclic voltammetry of **1-3SbF$_6$** in CH_2Cl_2 is characterized by electrochemically irreversible waves (Figure S12, Table 3). Such an electrochemical behavior is difficult to interpret and hinders a comparison between the electronic properties of the complexes.

FT-IR Spectroscopy of the CO Bound Adducts. FT-IR analyses of the Cu^I−CO adducts generated in situ by CO bubbling through CH_2Cl_2 solutions of the complexes show a ν(CO) of 2085 cm^{-1} for **1** and **2** and 2089 cm^{-1} for **3** (Table 3), which indicates that the tert-butyl group does not significantly improve the electron donating character in comparison with H. We conclude that the electronic properties of the Cu^I centers are only slightly modulated by the substituent in the aromatic ring of the ligand through the imine group conjugated to the arene moiety. It is also interesting to compare the values obtained for the CO adducts of **1**−**3** with the one described for $[Cu^I_2(m\text{-}XYL^{MeAN})]^{2+}$ (2085 cm^{-1}).[9] Surprisingly, the coincident CO stretching frequency suggests that the imine and the benzylic NMe group convey analogous electronic properties with respect to the copper ions.

O$_2$ Reactivity. Orange dicopper(I) complexes **1X**, **2X**, and **3X**, (X = ClO_4, CF_3SO_3, SbF_6, and BArF) are very reactive toward O_2 both in the solid state and in solution, rapidly turning green at room temperature upon exposure to air. When acetone, CH_2Cl_2, or THF solutions of the complexes are exposed to O_2 at cryogenic temperatures (−90 °C), new yellow metastable species **1(O$_2$)X**, **2(O$_2$)X**, and **3(O$_2$)X** develop. These species have common features in their UV−vis spectra characterized by two intense bands near 300 and 400 nm (Table S7). For the specific case of **1BArF** in THF, the resulting metastable species **1(O$_2$)BArF** is characterized

(36) Karlin, K. D.; Nasir, M. S.; Cohen, B. I.; Cruse, R. W.; Kaderli, S.; Zuberbühler, A. D. *J. Am. Chem. Soc.* **1994**, *116*, 1324−1336.

Scheme 3. Schematic Structure of **1**−**3(O₂)X** as Ascertained by Resonance Raman

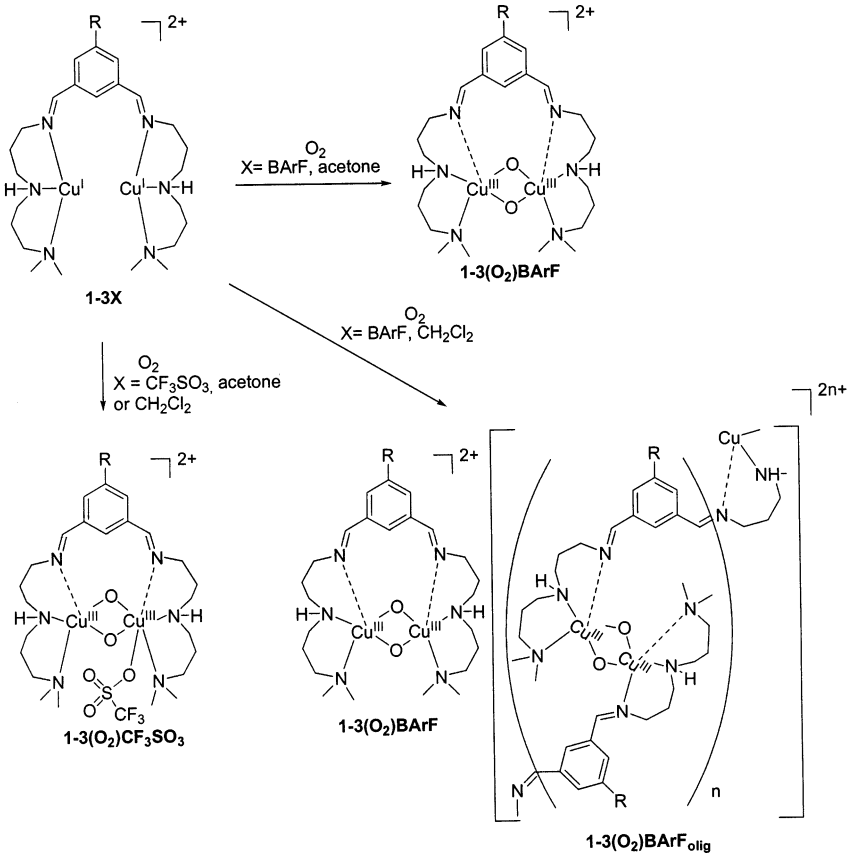

by $\lambda_{max} = 298$ nm, $\epsilon = 16\,000$ M^{-1} cm^{-1}, and $\lambda_{max} = 405$ nm, $\epsilon = 19\,000$ M^{-1} cm^{-1} (Figure 3). These features are indicative of a $Cu^{III}_2(\mu\text{-}O)_2$ core and closely resemble those of the structurally related $[Cu^{III}_2(\mu\text{-}O)_2(\text{m-XYL}^{MeAN})]^{2+}$ (as ascertained by DFT methods) recently described by us.[9] It is well-established that $Cu^{III}_2(\mu\text{-}O)_2$ cores tend to be close in energy to their $Cu^{II}_2(\mu\text{-}\eta^2\text{:}\eta^2\text{-}O_2)$ isomer form, and that interconversion between the two isomeric forms is fast because of a small energy barrier.[37,38] Nevertheless, no evidence for the presence of the $Cu^{II}_2(\mu\text{-}O_2)$ isomer form was observed by UV−vis spectroscopy, irrespective of complex **1X**−**3X**, solvent (CH_2Cl_2, acetone, THF), or counterion (CF_3SO_3, SbF_6, ClO_4, BArF) employed, thus indicating that for the present system the $Cu^{II}_2(\mu\text{-}O_2)$ isomer is significantly higher in energy (vide infra). Small but significant differences in the λ_{max} and extinction coefficients were observed depending on counterion, ligand, and solvent, suggesting that although the $Cu^{III}_2(\mu\text{-}O)_2$ core is present in all the cases, the complete structure and stability may be somewhat dependent on solvent and/or counterion. This aspect was further clarified by resonance Raman spectroscopy (vide infra).

Bis-oxo species **1(O₂)X**, **2(O₂)X**, and **3(O₂)X** are highly unstable, and rapid decay is observed even at −90 °C, precluding further characterization except by resonance Raman spectroscopy in liquid-N_2-frozen solutions. Their decay was dependent on the counterion, with the oxygenated complexes for X = BArF found to be somewhat more stable than those for X = CF_3SO_3.

Resonance Raman Characterization of the O_2 Adducts. Resonance Raman characterization of **1(O₂)X**, **2(O₂)X**, and **3(O₂)X**, X = BArF and CF_3SO_3, was performed on liquid-N_2-frozen samples. These complexes were chosen on the basis of the different coordinating abilities of CF_3SO_3 and BArF counterions. While there are several examples in Cu/O_2 chemistry where CF_3SO_3 anions coordinate to $Cu^{III}_2(\mu\text{-}O)_2$ cores,[39,40] BArF anions are well-established as noncoordinating anions, even in the presence of highly electrophilic metal centers.[41] Resonance Raman analysis of **1(O₂)X**, **2(O₂)X**, and **3(O₂)X** substantiates their assignments as $Cu^{III}_2(\mu\text{-}O)_2$ species[42,43] but also provides evidence for an unexpected complexity in the structures of the oxygenated products that depend on the solvent and counterion employed (Scheme 3). Resonance Raman spectra of frozen dichloromethane solutions of **1(O₂)CF₃SO₃**−**3(O₂)CF₃SO₃** with $\lambda = 407$ nm laser excitation exhibit a single resonance

(37) Tolman, W. B. *Acc. Chem. Res.* **1997**, *30*, 227−237.
(38) Halfen, J. A.; Mahapatra, S.; Wilkinson, E. C.; Kaderli, S.; Young, V. G., Jr.; Que, L., Jr.; Zuberbühler, A. D.; Tolman, W. B. *Science* **1996**, *271*, 1397−1400.
(39) Aboelella, N. W.; Lewis, E. A.; Reynolds, A. M.; Brennessel, W. W.; Cramer, C. J.; Tolman, W. B. *J. Am. Chem. Soc.* **2002**, *124*, 10660−10661.
(40) Ottenwaelder, X.; Rudd, D. J.; Corbett, M. C.; Hodgson, K. O.; Hedman, B.; Stack, T. D. P. *J. Am. Chem. Soc.* **2006**, *128*, 9268−9269.
(41) Brookhart, M.; Grant, B.; Volpe, A. F. J. *Organometallics* **1992**, *11*, 3920−3922.
(42) Holland, P.; Cramer, C. J.; Wilkinson, E. C.; Mahapatra, S.; Rodgers, K. R.; Itoh, S.; Taki, M.; Fukuzumi, S.; Que, L., Jr.; Tolman, W. B. *J. Am. Chem. Soc.* **2000**, *122*, 792−802.
(43) Que, L., Jr.; Tolman, W. B. *Angew. Chem., Int. Ed.* **2002**, *41*, 1114−1137.

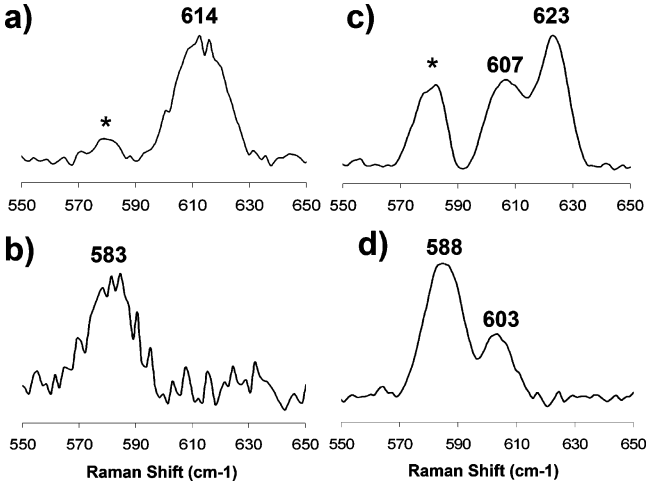

Figure 4. Resonance Raman spectra of 1 mM solution in CH_2Cl_2 of (a) **1(O₂)CF₃SO₃**, (b) **1(¹⁸O₂)CF₃SO₃**, (c) **1(O₂)BArF**, and (d) **1(¹⁸O₂)-BArF**.

Raman enhanced peak at $\nu \sim 613$ cm^{-1}, which experiences a $[\Delta^{18}O_2-{}^{16}O_2] \sim 30$ cm^{-1} downshift when $^{18}O_2$ is employed in the oxygenation reaction (Figures 4 and 5 and Table 4). When the same oxygenation reactions were carried out with **1BArF**−**3BArF** in CH_2Cl_2, the resonance Raman spectra of the complexes became more complicated, showing more than one vibrational feature. For instance, when **1BArF** was oxygenated in CH_2Cl_2, two sets of signals at $\nu \sim 623$ cm^{-1} ($[\Delta^{18}O_2-{}^{16}O_2] = 20$ cm^{-1}) and $\nu \sim 607$ cm^{-1} ($[\Delta^{18}O_2-{}^{16}O_2] = 19$ cm^{-1}) were observed. Unlike in the case of **1-(O₂)CF₃SO₃**−**3(O₂)CF₃SO₃**, the energies of these features were slightly dependent on the complex employed (Table 4 and Figures 4 and 5). There was no evidence for the $\nu = 613$ cm^{-1} peak observed in **1(O₂)CF₃SO₃**−**3(O₂)CF₃SO₃** in the spectra of the BArF derivatives, indicating that the counterion influences the structure of the bis-oxo core. The relative intensities of the two peaks observed in the BArF derivatives depended on the complex concentration, with the lower energy features gaining in intensity upon dilution of the starting dicopper(I) complex at the expense of the higher energy peak (Figure 5). We interpret this behavior as the result of a competition between intramolecular and intermolecular O_2 binding. Analogous competitive reactions in other xylyl-linked dicopper complexes have been observed by Karlin et al. and Tolman et al.[44,45] Interestingly, when **1BArF**−**3BArF** were oxygenated in acetone, only a feature at 600−602 cm^{-1} was observed in the spectra (Figure S13), indicating that only one product is formed in this solvent, which is assigned to the product resulting from intramolecular binding. This observation suggests that the acetone solvent has a similar effect as the triflate anion in CH_2Cl_2, promoting the intramolecular binding of dioxygen to the dicopper complex.

The vibrational properties in CH_2Cl_2 of the BArF containing complexes differ from those associated with **1(O₂)-CF₃SO₃**−**3(O₂)CF₃SO₃** and **1X**−**3X** (X = CF_3SO_3 or BArF) in acetone. These observations demonstrate that X and/or solvents with coordinating abilities play a role in determining the structures of **1(O₂)X**−**3(O₂)X**. Precedence for CF_3SO_3 binding to the Cu_2O_2 core has been unambiguously documented by Tolman et al. and Stack et al.[39,40] The binding role of the triflate group is supported by DFT calculations (vide infra). On the other hand, the noncoordinating BArF counterion cannot interact with the Cu_2O_2 core. Without the directing role of the triflate or acetone, inter- and intramolecular O_2 interactions become competitive.

DFT Characterization of Bis-μ-oxo Complexes 1(O₂)-X−3(O₂)X (X = CF₃SO₃ and BArF). Because of the inherent thermal instability of the bis-oxo complexes **1(O₂)-X**−**3(O₂)X** (X = CF_3SO_3 and BArF), further insight into their structures was obtained via DFT methods. Particularly important aspects of this study are (a) the chemical identities and structural parameters of the O_2 adducts, and (b) the relative stability of the $Cu^{III}_2(\mu\text{-O})_2$ form versus the $Cu^{II}_2(\mu\text{-}\eta^2\text{:}\eta^2\text{-O}_2)$ isomer.

Calculated structures of $\mathbf{[1(O_2)]^{2+}}$ for $Cu^{II}_2(\mu\text{-}\eta^2\text{:}\eta^2\text{-O}_2)$ and $Cu^{III}_2(\mu\text{-O})_2$ isomers are depicted in Figure 6, and the structural data are collected in Tables 5 and 6 (the corresponding labeling scheme is shown in Figure 6). Analogous structures calculated for $\mathbf{[2(O_2)]^{2+}}$ and $\mathbf{[3(O_2)]^{2+}}$ are depicted in Figure S14. Calculations indicate the presence of a single minimum for the $Cu^{II}_2(\mu\text{-}\eta^2\text{:}\eta^2\text{-O}_2)$ isomers, but two stable structures are obtained for each $Cu^{III}_2(\mu\text{-O})_2$ form that differ in the number of Cu−N bonds (two or three). For reasons of clarity, only the more stable $Cu^{III}_2(\mu\text{-O})_2$ form for $\mathbf{[1(O_2)]^{2+}}$ is shown in Figure 6.

In each case, the $Cu^{III}_2(\mu\text{-O})_2$ isomer is significantly more stable than the corresponding $Cu^{II}_2(\mu\text{-}\eta^2\text{:}\eta^2\text{-O}_2)$ peroxo isomer (from 20.2 to 35.6 kJ·mol^{-1}). This result justifies the sole observation of the former oxygen adduct in our experiments. As can be seen in Figure 6, the ligand adopts a quite different conformation in the $Cu^{II}_2(\mu\text{-}\eta^2\text{:}\eta^2\text{-O}_2)$ and $Cu^{III}_2(\mu\text{-O})_2$ isomers. One may wonder whether such a difference helps to explain the relative stability of the two isomers. To solve this question, we have calculated the energy of the ligands frozen at the geometry they have in the $Cu^{II}_2(\mu\text{-}\eta^2\text{:}\eta^2\text{-O}_2)$ and $Cu^{III}_2(\mu\text{-O})_2$ isomers. It has been found that the ligand at the $Cu^{III}_2(\mu\text{-O})_2$ geometry is 51.0 kJ·mol^{-1} more stable than the same ligand in the conformation of the $Cu^{II}_2(\mu\text{-}\eta^2\text{:}\eta^2\text{-O}_2)$ isomer. The reason for the large stability of the ligand in the $Cu^{III}_2(\mu\text{-O})_2$ isomer conformation is the additional flexibility that the ligand has in this species because two of the imine N atoms remain noncoordinated. It can be concluded that the different conformation of the two ligands in the $Cu^{II}_2(\mu\text{-}\eta^2\text{:}\eta^2\text{-O}_2)$ and $Cu^{III}_2(\mu\text{-O})_2$ isomers is in part responsible for the larger stability of the $Cu^{III}_2(\mu\text{-O})_2$ isomer. Therefore, one may expect that for less flexible ligands the relative stability of the $Cu^{II}_2(\mu\text{-}\eta^2\text{:}\eta^2\text{-O}_2)$ and $Cu^{III}_2(\mu\text{-O})_2$ isomers can be reversed. And this is indeed what is found in a previous study for the calculated O_2 adducts of $[Cu^{I}_2(sb2m)]^{2+}$, $[Cu^{I}_2(sb3m)]^{2+}$, and $[Cu^{I}_2(Me3m)]^{2+}$ (see Scheme 1).[46]

(44) Pidcock, E.; Obias, H. V.; Zhang, C. X.; Karlin, K. D.; Solomon, E. I. *J. Am. Chem. Soc.* **1998**, *120*, 7841−7847.
(45) Mahapatra, S.; Kaderli, S.; Llobet, A.; Neuhold, Y.-M.; Palanche, T.; Halfen, J. A.; Young, V. G., Jr.; Kaden, T. A.; Que, L.; Zuberbuehler, A. D.; Tolman, W. B. *Inorg. Chem.* **1997**, *36*, 6343−6356.

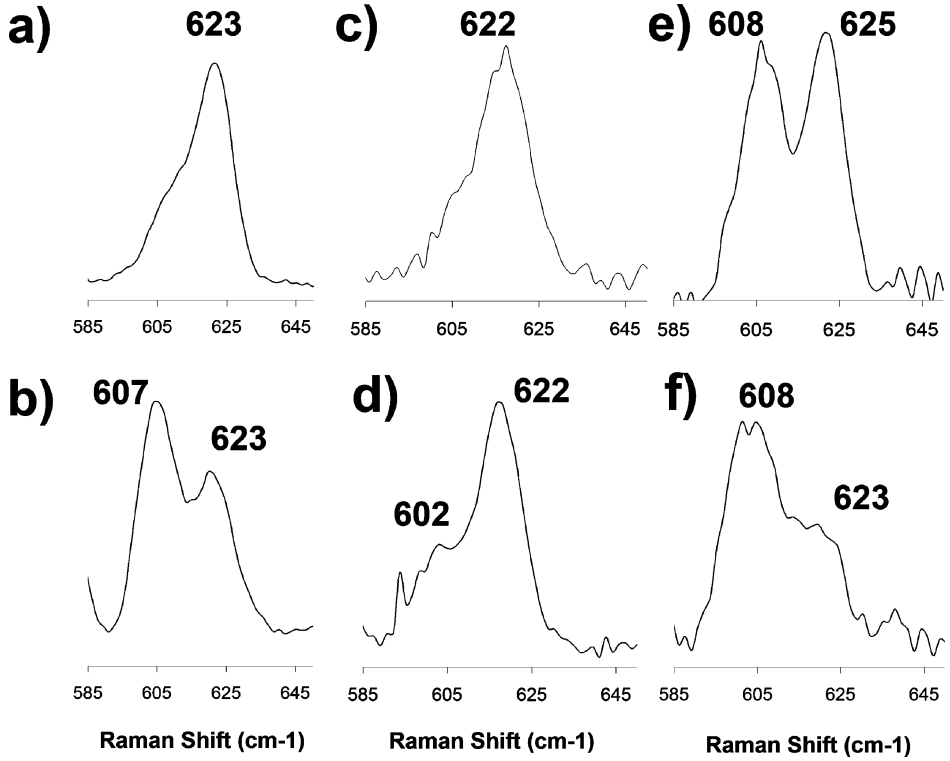

Figure 5. Resonance Raman spectra in CH_2Cl_2 of (a) 20 mM **1(O₂)BArF**, (b) 0.2 mM **1(O₂)BArF**, (c) 20 mM **2(O₂)BArF**, (d) 0.2 mM **2(O₂)BArF**, (e) 20 mM **3(O₂)BArF**, and (f) 0.2 mM **3(O₂)BArF**.

Table 4. Spectroscopic Properties of Dicopper Complexes **1(O₂)X**−**3(O₂)X**

	UV−vis λ_{max}, nm (ϵ,[a] M^{-1} cm^{-1})		ν (cm^{-1}) [$\Delta^{18}O_2-{}^{16}O_2$]	
complex	CH_2Cl_2	acetone	CH_2Cl_2	acetone
1(O₂)BArF	407 (13000)	410 (13000)	623 [20]	601
	295 (14000)		607 [19]	
2(O₂)BArF	407 (9000)	407 (7000)	622 [28]	602
3(O₂)BArF	406 (6000)	406 (4000)	625 [27]	600
			608 [26]	
1(O₂)CF₃SO₃	402 (11000)	408 (17000)	614 [31]	602
2(O₂)CF₃SO₃	402 (10000)	406 (6000)	613 [28]	600
	295 (14000)			
3(O₂)CF₃SO₃	403 (6000)	403 (7000)	612 [29]	601

[a] Because of fast decomposition, extinction coefficients are lower limit values.

The structures of the $Cu^{III}_2(\mu\text{-}O)_2$ isomers of $\mathbf{[1(O_2)]^{2+}}$−$\mathbf{[3(O_2)]^{2+}}$ are characterized by a nearly planar Cu_2O_2 core, with Cu ions adopting a distorted square-planar coordination geometry. Selected average distances are Cu−N, 1.966 Å; Cu−O, 1.792 Å; O···O, 2.287 Å; and Cu···Cu, 2.754 Å; these are values that are within the range of those described for crystallographically characterized related species[38,39,47−50]

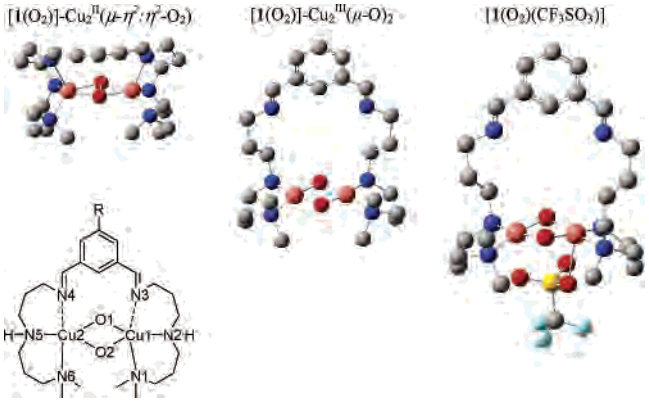

Figure 6. Structure of the Cu_2O_2 adducts obtained by DFT calculations, along with a labeling scheme. H atoms have been omitted for clarity (color code: Cu pink, N blue, C gray, O red, S yellow, F light blue).

and are especially similar to the compact bis-oxo cores described by Stack et al. for copper complexes containing alkylated diamines. Not unexpectedly, the imine N atoms are not coordinated, being placed at ∼4.8 Å from the Cu in a nearly apical position.

The most stable Cu^{III} species is stabilized with respect to the Cu^{II} species by 25.9, 20.2, and 35.6 kJ·mol^{-1} for $[\mathbf{1}(O_2)]^{2+}$, $[\mathbf{2}(O_2)]^{2+}$, and $[\mathbf{3}(O_2)]^{2+}$, respectively. Considering that the imine groups are bound to the Cu^{II} ion in the $Cu^{II}_2(\mu\text{-}\eta^2\text{:}\eta^2\text{-}O_2)$ but not in the $Cu^{III}_2(\mu\text{-}O)_2$ isomers, the larger energy difference calculated for $[\mathbf{3}(O_2)]^{2+}$ most likely arises from poorer stabilization of the Cu^{II} species by the electron-withdrawing nitro group. We substantiated this hypothesis by calculating the energy differences between $Cu^{II}_2(\mu\text{-}\eta^2\text{:}\eta^2\text{-}O_2)$ and $Cu^{III}_2(\mu\text{-}O)_2$ isomers for hypothetical complexes $[Cu_2O_2(^RL)]$, R = Cl and CH_3. The *p*-chloro and *p*-methyl

(46) Costas, M.; Ribas, X.; Poater, A.; Lopez-Valbuena, J. M.; Xifra, R.; Company, A.; Duran, M.; Solà, M.; Llobet, A.; Corbella, M.; Uson, M. A.; Mahia, J.; Solans, X.; Shan, X.; Benet-Buchholz, J. *Inorg. Chem.* **2006**, *45*, 3569−3581.
(47) Mahadevan, V.; Hou, Z.; Cole, A. P.; Root, D. E.; Lal, T. K.; Solomon, E. I.; Stack, T. D. P. *J. Am. Chem. Soc.* **1997**, *119*, 11996−11997.
(48) Hayashi, H.; Fujinami, S.; Nagatomo, S.; Ogo, S.; Suzuki, M.; Uehara, A.; Watanabe, Y.; Kitagawa, T. *J. Am. Chem. Soc.* **2000**, *122*, 2124−2125.
(49) Mahapatra, S.; Young, V. G., Jr.; Kaderli, S.; Zuberbühler, A. D.; Tolman, W. B. *Angew. Chem., Int. Ed.* **1997**, *36*, 130−133.
(50) Straub, B. F.; Rominger, F.; Hofmann, P. *Chem. Commun.* **2000**, 1611−1612.

Table 5. Structural Data of $[\mathbf{1(O_2)}]^{2+}-[\mathbf{3(O_2)}]^{2+}$ Optimized Structures[a]

	$[\mathbf{1(O_2)}]^{2+}$		$[\mathbf{2(O_2)}]^{2+}$		$[\mathbf{3(O_2)}]^{2+}$	
	$Cu^{II}_2(\mu\text{-}\eta^2\text{:}\eta^2\text{-}O_2)$	$Cu^{III}_2(\mu\text{-}O)_2$	$Cu^{II}_2(\mu\text{-}\eta^2\text{:}\eta^2\text{-}O_2)$	$Cu^{III}_2(\mu\text{-}O)_2$	$Cu^{II}_2(\mu\text{-}\eta^2\text{:}\eta^2\text{-}O_2)$	$Cu^{III}_2(\mu\text{-}O)_2$
Cu1Cu2	3.625	2.755	3.624	2.754	3.624	2.754
O1O2	1.436	2.287	1.436	2.287	1.437	2.287
Cu1N1	2.033	1.970	2.053	1.971	2.054	1.970
Cu1N2	2.046	1.963	2.027	1.962	2.018	1.962
Cu1N3	2.211	4.827	2.219	4.758	2.241	4.799
Cu2N4	2.227	4.827	2.216	4.758	2.222	4.798
Cu2N5	2.019	1.963	2.032	1.962	2.031	1.964
Cu2N6	2.058	1.970	2.050	1.971	2.047	1.970
Cu1O1	1.954	1.791	1.938	1.793	1.937	1.793
Cu1O2	1.949	1.794	1.960	1.792	1.960	1.792
Cu2O1	1.962	1.791	1.942	1.792	1.948	1.793
Cu2O2	1.935	1.794	1.958	1.792	1.958	1.792
Cu1O1Cu2	135.5	100.6	135.3	100.5	135.3	100.4
Cu1O2Cu2	137.9	100.4	138.2	100.4	137.8	100.4

[a] Distances in Å, angles in deg. Atom labels are given in Figure 6.

Table 6. Structural Data of $[\mathbf{1(O_2)CF_3SO_3}]^{+}-[\mathbf{3(O_2)CF_3SO_3}]^{+}$ Optimized Structures[a]

	$[\mathbf{1(O_2)CF_3SO_3}]^{+}$	$[\mathbf{2(O_2)CF_3SO_3}]^{+}$	$[\mathbf{3(O_2)CF_3SO_3}]^{+}$
Cu1−Cu2	2.703	2.704	2.703
O1−O2	2.289	2.289	2.288
Cu1−N1	1.980	1.980	1.980
Cu1−N2	1.969	1.969	1.970
Cu1−N3	4.906	4.916	4.930
Cu2−N4	4.871	4.880	4.895
Cu2−N5	1.969	1.969	1.971
Cu2−N6	1.972	1.972	1.971
Cu1−O1	1.796	1.796	1.796
Cu1−O2	1.805	1.805	1.805
Cu2−O1	1.788	1.788	1.788
Cu2−O2	1.794	1.795	1.795
Cu1−O (OTf)	2.526	2.527	2.520
Cu1−O1−Cu2	97.9	98.0	97.9
Cu1−O2−Cu2	97.4	97.4	97.3

[a] Distances in Å, angles in deg. Atom labels are given in Figure 6.

substituents give energy differences of 29.6 and 23.0 kJ·mol^{-1}, respectively, between peroxo and bis-oxo species, also reinforcing the idea that electronic effects have an impact in the relative stability of these isomers.

Structures of $[\mathbf{1(O_2)CF_3SO_3}]^{+}-[\mathbf{3(O_2)CF_3SO_3}]^{+}$ were also calculated by introducing a CF_3SO_3 group bound to the Cu_2O_2 core. Optimization routines converge to a single stable structure where the triflate ion is weakly bound ($d_{Cu-O} \sim 2.524(1)$ Å) in a terminal mode to a single Cu ion (Figure 6, Table 6). The binding of the triflate group results in a "butterfly" bending of the Cu_2O_2 core, which leads to ~0.05 Å shorter Cu···Cu distances, but significant differences in the Cu−O distances are not found. Comparable structural parameters in triflate bound $Cu^{III}_2(\mu\text{-}O)_2$ cores have been described by Tolman et al. and Stack et al. on the basis of crystallographic[39] and X-ray absorption spectroscopic analysis.[47,51]

Calculations for **1(O$_2$)BArF−3(O$_2$)BArF** complexes predict the a_g "breathing" mode to appear at $\nu \sim 638$ ($[\Delta^{18}O_2-{}^{16}O_2] = 31$), 640 ($[\Delta^{18}O_2-{}^{16}O_2] = 32$), and 640 ($[\Delta^{18}O_2-{}^{16}O_2] = 31$) cm^{-1}, respectively. An estimation of the energy of this vibrational mode in a bimolecular $\{[Cu^{III}_2(\mu\text{-}O)_2{}^{H}L]_2\}$ species, where the bis-oxo core is formed between two different copper complexes, has been done computationally. The intermolecular interaction between two **1** molecules was simplified due to computational cost by replacing the phenyl ring by a H atom. The computed value of 645 cm^{-1} shows an increase of 7 cm^{-1} for the intermolecular complex, which is consistent with the experimental observations, thus reinforcing the hypothesis that the observed higher frequency vibration corresponds to species where O_2 binding occurs intermolecularly.

Kinetic Studies on O$_2$ Binding. Kinetic studies on the oxygenation of **1BArF** and **1CF$_3$SO$_3$** in acetone were performed under pseudo-first-order conditions (large excess of dioxygen with respect to dicopper complex) over the temperature range from −80 to −20 °C by stopped-flow spectroscopy. The oxygenation rates of **1CF$_3$SO$_3$** were essentially the same as the oxygenation rates of the **1BArF** complex, so no obvious effect of the anion was observed, and therefore, detailed stopped-flow studies were not performed with **1CF$_3$SO$_3$**. Examples of the oxygenation kinetics data are included as Supporting Information. The oxygenation of **1BArF** in acetone proceeds with rapid accumulation of the bis-μ-oxo species **1(O$_2$)BArF** (over ca. 200 ms at −40 °C) immediately followed by its decomposition. Reproducible kinetic parameters could be obtained for this biphasic reaction. The oxygenation of **1BArF** proceeded as essentially 1-exponential reactions on the stopped-flow time scale, as the decomposition of **1(O$_2$)BArF** was much slower than oxygen binding to **1BArF**.

The observed pseudo-first-order rate constants for **1(O$_2$)BArF** formation were independent of the concentration of **1BArF** but increased linearly with dioxygen concentration (Figures S21−S22). Consequently, the oxygenation of complex **1BArF** is a second-order process (first-order in dicopper complex and first-order in O_2):

$$-\frac{d[LCu_2]}{dt} = k_{obs}[LCu_2] = k[O_2][LCu_2] \qquad (5)$$

On the basis of previously described kinetic analyses on the oxygenation of copper complexes,[4,52] and given the rather

(51) Mahadevan, V.; DuBois, J. L.; Hedman, B.; Hodgson, K. O.; Stack, T. D. P. *J. Am. Chem. Soc.* **1999**, *121*, 5583−5584.

(52) Karlin, K. D.; Kaderli, S.; Zuberbühler, A. D. *Acc. Chem. Res.* **1997**, *30*, 139−147.

Table 7. Kinetic Parameters for the Oxygenation of **1BArF** and Related Complexes

complex	k_{ox}, $M^{-1}\cdot s^{-1}$ (183 K)	$\Delta H^{\ddagger}$, $kJ\cdot mol^{-1}$	$\Delta S^{\ddagger}$, $J\cdot K^{-1}\cdot mol^{-1}$	ref
1BArF	$3.84(6) \times 10^3$ [a]	4.9(1)	−148(1)	this work
$[Cu^I_2(m\text{-}XYL^{MeAN})]^{2+}$	3.2[a]	9.5	−175	9
$[Cu^I_2(XYL\text{-}H)]^{2+}$	1.58×10^3 [b]	2.1	−174	55
$[Cu^I_2(MeL66)]^{2+}$	7.72×10^{-2} [c]	40.4	−41.4	56
$[Cu^I_2(m\text{-}Xyl^{iPr4})(CH_3CN)_2]^{2+}$	2.46[a]	39.4	−30	45
$[Cu^I(AN)]^+$	2.7×10^4 [d]	−9.9	−210	33
$[Cu^I(MeAN)]^+$	690[d]	−27	−335	33

[a] 193 K. [b] 253K. [c] Calcd from reported kinetic parameters. [d] $M^{-2}\ s^{-1}$.

flexible structure of the initial dicopper complex **1BArF**, which makes concerted O_2 binding to the two Cu^I sites unlikely, a minimum fundamental scheme for the formation of **1(O$_2$)BArF** would be

$$LCu^I_2 + O_2 \underset{k_2}{\overset{k_1}{\rightleftharpoons}} LCu^ICu^{II}O_2^{-\bullet} \xrightarrow{k_2} LCu^{II}{}_2O_2 \qquad (6)$$

In this scheme, a mixed valence Cu^ICu^{II-}superoxide species appears as a first elementary step, although no evidence for such species has yet been obtained neither by UV−vis spectroscopy nor from kinetic analysis. Activation parameters of the oxygenation reactions were determined from a linear Eyring plot (Figure S15, Table S3). A small activation enthalpy ($\Delta H^{\ddagger} = 4.9 \pm 0.5$ kJ·mol^{-1}) and a large negative activation entropy ($\Delta S^{\ddagger} = -148 \pm 5$ J·K^{-1}·mol^{-1}) typical of associative reactions are obtained.[53] The determined rate-law for the oxygenation of **1BArF** is consistent with two different mechanistic scenarios: (a) O_2 binding to the first copper center may be the rate-determining step. In such case, k_{obs} is dominated by k_1. (b) the second mechanistic picture involves reversible reaction of O_2 with **1BArF** to generate a putative superoxo $Cu^ICu^{II}O_2^-$ species in a left-lying pre-equilibrium process, followed by intramolecular collapse into the final dinuclear **1(O$_2$)BArF** structure. Activation parameters may then result from a combination of three reactions ($k_{obs} = k_1k_{-1}{}^{-1}k_2$). Under this scenario, k_2 could overcome an unfavorable pre-equilibrium process (k_1/k_{-1}). O_2 binding in this scheme will not only be determined by the particular affinity of a Cu^I center to undergo $1e^-$ oxidation by O_2 (either via an inner or outer sphere mechanism) but also by the ability of the two Cu^I ions to act synergistically, that is, to be able to attain the right Cu···Cu distance and relative orientation in order to promote O_2 binding. The latter scenario finds support in basic thermodynamic considerations of O_2 reduction. While $1e^-$ reduction to the superoxide level by a transition metal ion is usually an energetically uphill process, $2e^-$ reduction tends to be favorable.[54] Discerning between the two mechanistic scenarios may be complicated. We have recently demonstrated that dicopper complexes having nearly analogous structural and electronic properties as **1BArF** exhibit dramatic differences in their reactivity toward O_2, which could be explained on the basis of the relative ability of the different dicopper complexes to place the two metal ions in close proximity, so that synergistic O_2 binding occurs.[9] Structural similarity between $[Cu^I_2(m\text{-}XYL^{MeAN})]^{2+}$ and **1BArF** suggests that the same mechanistic scheme applies.

In addition, comparison with the kinetic parameters determined for the oxygenation of several xylyl-linked dicopper complexes (Table 7) reveals several interesting points that further strengthen the previous discussion: the low activation enthalpy and the large activation entropy associated to **1BArF** oxygenation are very similar to those of the XYL-H system described by Karlin.[55] The related bis-benzimidazole system reported by Casella (MeL66)[56] and the xylyl bridged triazacyclononane complex ($m\text{-}XYL^{ipr4}$) described by Tolman[45] are characterized by a larger activation enthalpy and a less negative activation entropy. For the former, the larger activation barrier has been proposed to arise from the slow conformational rearrangement of the bulky *N*-methyl-benzimidazole, and also from the loss of favorable aromatic ring stacking interactions occurring in the Cu^I_2 complex upon O_2 binding.[56] For the latter, activation parameters probably reflect that O_2 binding requires ligand (nitrile) dissociation.[45] Karlin's and Casella's complexes contain three-coordinate copper sites and rather soft heterocyclic nitrogen ligands, forming six-membered ring metallocycles, but Tolman's complexes contain four-coordinate copper ions and hard aliphatic amine nitrogen ligands. A direct structure−oxygenation rate correlation on these complexes appears to be thus unpredictable. O_2 binding in these complexes leads to μ-η^2:η^2 peroxo dicopper type of species, and unlike **1BArF**, the reaction is reversible. On the other hand, mononuclear copper complexes $[Cu^I(AN)]^+$ and $[Cu^I(MeAN)]^+$ containing aliphatic triamine ligands exhibit different rate laws, and significantly different activation parameters.[33] Interestingly, in these closely structurally related complexes, the second-order dependence of the oxygenation rate on copper complex kinetically requires a fast and left-lying pre-equilibrium (no superoxide intermediate is detected). Negative activation enthalpies further support the proposal that O_2 binding constants result from a combination of rate constants rather than a single rate-determining step.

Finally, it is surprising that xylyl bridged $[Cu^I_2(m\text{-}XYL^{MeAN})]^{2+}$ and **1BArF** differ by more than 3 orders of magnitude in their oxygenation rates.[9] Kinetic analysis indicates that this difference originates both from a smaller activation enthalpy and a less negative activation entropy.

(53) Tobe, M. L.; Tobe, M. L.; Burgess, J. *Inorganic Reaction Mechanisms*, 1st ed.; Prentice Hall: London, 1999.
(54) Sawyer, D. T. *Oxygen Chemistry*; Oxford University Press: New York, 1991.
(55) Becker, M.; Schindler, S.; Karlin, K. D.; Kaden, T. A.; Kaderli, S.; Palanché, T.; Zuberbühler, A. D. *Inorg. Chem.* **1999**, *38*, 1989−1995.
(56) Palavicini, S.; Granata, A.; Monzani, E.; Casella, L. *J. Am. Chem. Soc.* **2005**, *127*, 18031−18036.

Indeed, to the best of our knowledge O_2 binding to **1BArF** is the fastest reported in the literature for an m-XYL system, with the single exception of $[Cu^I_2(XYL\text{-}O)]^+$,[57] where the two copper ions are highly preorganized by a phenoxide bridge. We suggest that this fast reactivity may arise from a combination of factors: (a) the relatively higher preorganization conferred by the more rigid imine N group in comparison with tertiary amines, (b) a possible hemilability of the imine group that may lower the coordination number of the Cu ion, enhancing its reactivity, and (c) the presence of the NH group which may stabilize O_2 binding to the first Cu ion via H-bonding or via better stabilization of the Cu^{II} or Cu^{III} oxidation state, as described by Meyerstein.[58]

Characterization of the Final Products. Species **1−3(O$_2$)X** are unstable even at −80 °C and rapidly decay to Cu^{II} final products, as indicated by the presence of weak absorptions at $\lambda_{max} \sim 600$ nm, ϵ/Cu ~ 100 M^{-1}/cm^{-1}. Several attempts were made to crystallize out any of the decayed species, but all proved unsuccessful. The chemical composition of the decayed products was therefore determined by acid decomposition of the ligand and analysis of the aromatic dialdehyde. Attempts to extract the cupric ions by aqueous ammonia treatment led to intractable mixtures. However, the acidic workup allowed us to recover the corresponding dialdehyde without any evidence that aromatic hydroxylation has occurred. Therefore, we conclude that thermal decay of **1(O$_2$)X−3(O$_2$)X** does not lead to arene hydroxylation.

1(O$_2$)BArF Decomposition Kinetics. The decomposition of **1(O$_2$)BArF** in acetone was investigated by stopped-flow methods. Decomposition rates of **1(O$_2$)BArF** in the temperature range −40 to −10 °C could be satisfactorily fitted to a single-exponential function. Activation parameters determined by least-squares fit from the Eyring equation (Figure S16) are $\Delta H^{\ddagger} = 60 \pm 1$ kJ·mol^{-1} and $\Delta S^{\ddagger} = -9 \pm 5$ J·mol^{-1}·K^{-1}. The activation enthalpy of **1(O$_2$)BArF** is consistent with the values obtained for the decomposition of a number of bis-μ-oxo complexes, via oxidative dealkylation of ligand backbones.[4] However, the small activation entropy is somewhat more uncommon. We conclude that the **1(O$_2$)BArF** thermal decomposition likely involves oxidative dealkylation of the aliphatic arms. However, attempts to recover the triamine, after acidic workup, have proven unsuccessful.

Conclusion. A new family of dicopper(I) complexes with Schiff-base ligands containing two tridentate binding sites linked by a xylyl spacer has been prepared and characterized. The electronic properties of the Cu^I ions in these complexes are only slightly modulated by the type of substitution (^{t}Bu, H, NO_2) in the fourth position of the aromatic linker. The complexes contain three coordinate Cu^I sites both in the solid state and in solution that exhibit fast reactivity toward O_2. Unlike previously studied dicopper(I) complexes containing Schiff-base ligands, which exhibit O_2 reactivity without accumulation of any reaction intermediate, well-defined but metastable $Cu^{III}_2(\mu\text{-}O)_2$ species **1−3(O$_2$)X** can be observed at low temperature and spectroscopically characterized in the reactions of **1−3X** (X = CF_3SO_3, SbF_6, ClO_4, and BArF) with O_2. The core structures of such species have been established by resonance Raman spectroscopy and shown to depend on the solvent and counterion; yet, no evidence for the $Cu^{II}_2(\mu\text{-}\eta^2\text{:}\eta^2\text{-}O_2)$ isomer has been found. The structures of **1−3(O$_2$)X** have also been studied by DFT methods, which also substantiate the higher stability of the bis-oxo species. Thermal decay of **1−3(O$_2$)X** does not result in aromatic self-hydroxylation, presumably because the arene ring is positioned far from the Cu_2O_2 core, as shown by the DFT calculations. A kinetic study of the reaction between the dicopper(I) complexes and O_2 reveals that the reaction is unexpectedly fast (more than 3 orders of magnitude faster than the related Cu^I complex $[Cu^I_2(m\text{-}XYL^{MeAN})]^{2+}$ with peralkylated amine ligands). These results further support the idea that O_2 binding in these complexes is directed not via the affinity of a single Cu^I ion toward O_2, but instead by their ability to promote a synergistic actuation of two Cu^I ions, and by a rather thermodynamically stable $Cu^{III}_2(\mu\text{-}O)_2$ core that forms upon Cu_2:O_2 interaction. The ability of these species to oxidize exogenous substrates will be the focus of our upcoming studies.

Acknowledgment. Financial support from MCYT of Spain through Projects CTQ2006-05367/BQU to M.C., CTQ2005-08797-C02-01 to M.S., and CTQ2006-01080 to T.P.; from NIH (GM-38767 to L.Q.); and from the US Department of Energy, Office of Basic Energy Sciences (DE-FG02-06ER15799 to E.R.-A.). A.C. and L.G. thank MEC for Ph.D. grants.

Supporting Information Available: Electrochemical, NMR, and UV−vis characterization of the complexes reported in this work. Details on the crystallographic characterization of **2ClO$_4$** and **3BArF**. DFT calculated structures of **2(O$_2$)**, **2(O$_2$)CF$_3$SO$_3$**, **3(O$_2$)**, and **3(O$_2$)CF$_3$SO$_3$**. Kinetic analysis details of the reaction of **1BArF** with O_2. This material is available free of charge via the Internet at http://pubs.acs.org.

IC0701108

(57) Cruse, R. W.; Kaderli, S.; Karlin, K. D.; Zuberbühler, A. D. *J. Am. Chem. Soc.* **1988**, *110*, 6882−6883.
(58) Golub, G.; Cohen, H.; Paoletti, P.; Bencini, A.; Bertini, L. M.; Meyerstein, D. *J. Am. Chem. Soc.* **1995**, *117*, 8353−8361.